



UNIVERSITÉ
DE GENÈVE

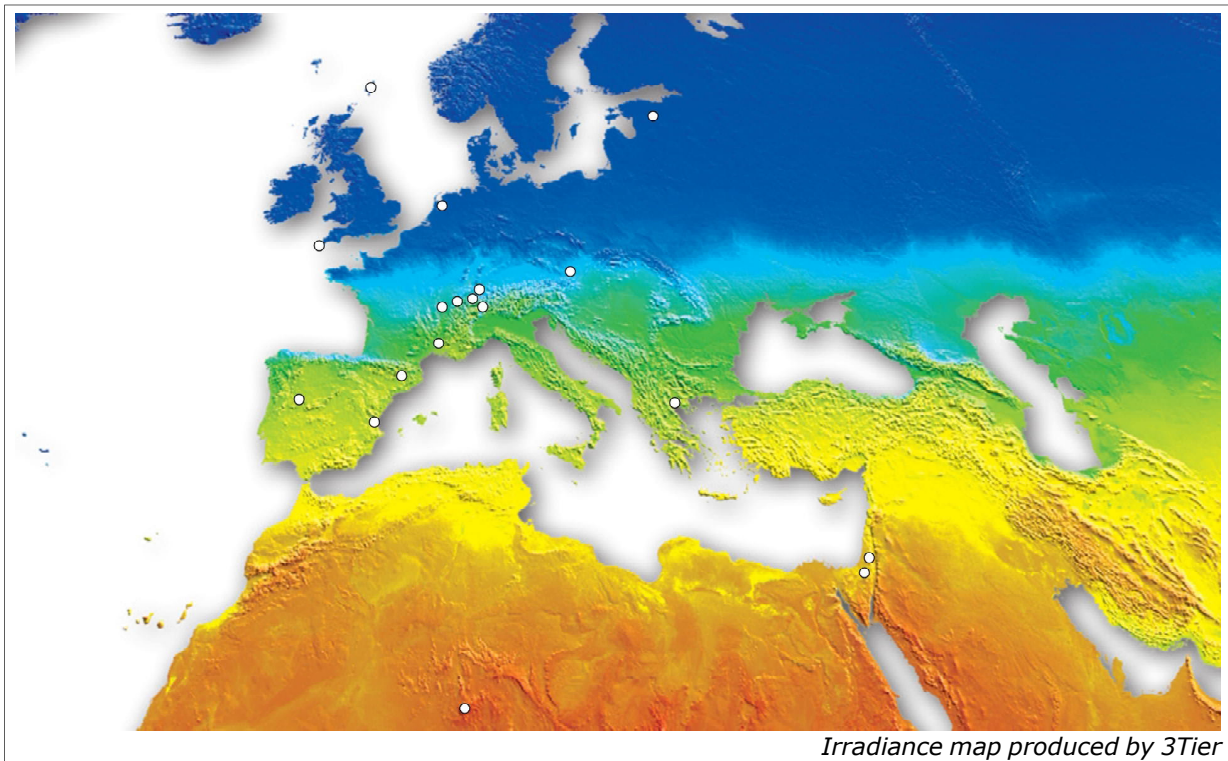
INSTITUT DES SCIENCES
DE L'ENVIRONNEMENT



International
Energy Agency

*Five satellite products deriving
beam and global irradiance validation
on data from 23 ground stations*

Pierre Ineichen
University of Geneva
February 2011



Five satellite products deriving beam and global irradiance validation on data from 23 ground stations

Pierre Ineichen
University of Geneva
February 2011

Abstract

Models converting satellite images into the different radiation components become increasingly performing and give often better estimation of the solar irradiance availability than ground measurements if the station is not situated in the near vicinity of the application.

Five different satellite products deriving both global and beam irradiance are validated against data from 23 ground sites. The main conclusions are:

- the global irradiance is retrieved with a negligible bias and an average standard deviation around 16% for the best algorithm. For the beam irradiance, the bias is around several percents, and the standard deviation around 35%,
- the main deviation comes from the knowledge of the aerosol optical depth,
- the high latitude sites give not poorer results than the other sites,

The interannual variability of the irradiance conditions, the lack of independent ground measurements such as aerosol data, the difficulty to assess the exact calibration of the ground data, and the choice of a specific year to carry out the validation, conduct to results that give good indications, but from which it is difficult to draw general conclusions.

1. Introduction

Models converting satellite images into the different radiation components become increasingly performing and give often better estimation of the solar irradiance availability than ground measurements if the station is not situated in the near vicinity of the application (Zelenka, 1999). If the global irradiance can be derived with a good accuracy, it is more difficult for the beam component and the dispersion of the models is higher.

The aim of the present study is to validate and compare five different products deriving the global and beam irradiance components from meteorological satellite images. It is a complement to a previous study conducted by the author (Ineichen 2009) on products from Eumetsat Satellite Application Facilities (SAF). These algorithmes are derived by GeoModel in Bratislava (SolarGis), Helioclim Soda (heliosat 3v3), 3Tier company in the United States, University of Oldenburg (EnMetSol-Solis and EnMetSol-Dumortier) and the IrSolAv company in Spain.

2. Ground data

The ground data used in the study are acquired at stations part of networks such as Baseline Solar Radiation Network (BSRN), Commission International de l'Eclairage (CIE), FluxNet network, Swiss Institute of Meteorology (ISM-Anetz) and World Radiation Data Center (WRDC). Data from 23 ground sites situated mainly on the European continent are used. The work is done on data covering the year 2006.

Beside the global horizontal irradiance G_h , half of the sites acquire the normal beam irradiance B_n . High precision instruments (WMO 2008) such as Kipp and Zonen CM10

Station	Country	Climate	D_h	B_n	latitude °	longitude °	altitude m	operated by
Cabauw	The Netherlands	temperate maritime	x	51.970	4.930	2	BSRN - KNMI	
Cambridge	United Kingdom	temperate maritime	x	50.220	-5.310	88	BSRN - Met Office	
Carpentras	France	mediterranean	x	44.080	5.060	100	BSRN - Météo France	
Davos Dorf	Switzerland	semi-continental alpin	x	46.810	9.840	1610	WRDC - Met Office	
El Saler	Spain	semi arid, warm summer		39.346	-0.319	10	FluxNet	
Geneva	Switzerland	semi-continental	x	46.199	6.131	420	CIE - UNIGE	
Jungfraujoch	Switzerland	high alpine	x	46.550	7.980	3571	CLIMAP - Météo Suisse	
Las Majadas	Spain	semi arid, warm summer		39.942	-5.773	260	FluxNet	
Lerwick	United Kingdom	cold oceanic	x	60.130	-1.180	82	BSRN - Met Office	
Locarno	Switzerland	warm temperate, humid		46.170	8.780	367	ANETZ - Météo Suisse	
Nantes	France	oceanic	x	47.150	-1.330	30	CIE - CSTB	
Payerne	Switzerland	moderate maritime/continental	x	46.820	6.950	490	BSRN - Météo Suisse	
Sede Boquer	Israel	dry steppe		30.867	34.767	457	BSRN - Met Office	
Sion	Switzerland	dry alpine		46.220	7.330	489	ANETZ - Météo Suisse	
Sonnblick	Austria	temperate alpine	x	47.050	12.950	3105	WRDC - ZAMG	
Tamanrasset	Algeria	hot, dry desert		22.780	5.520	1400	BSRN - Met Office	
Thessaloniki	Greece	mediterranean temperate	x	40.630	22.970	60	WRDC - Met Office	
Toravere	Estonia	cold humid	x	58.270	26.470	70	BSRN - EMHI	
Val Alinya	Spain	warm temperate, humid		42.152	1.449	1770	FluxNet	
Vaulx-en-Velin	France	semi-continental	x	45.780	4.930	170	CIE - ENTPE	
Wien / Hohe Warte	Austria	continental	x	48.250	16.350	203	WRDC - ZAMG	
Yatir Forest	Israel	hot arid		31.347	35.052	650	FluxNet	
Zürich	Switzerland	temperate atlantic		47.475	8.530	558	ANETZ - Météo Suisse	

ANETZ	MeteoSwiss network	CUEPE	Energy Group, UniGe
BSRN	Baseline Surface Radiation Network	EHMI	The Estonian Meteorological and Hydrological Institute
CIE	Commission Internationale pour l'Eclairage	ENTPE	Ecole Nationale des Mines de Paris
CLIMAP	MeteoSwiss Climate Maping application	KNMI	The Netherlands Institute of Meteorology
CSTB	Centre Scientifique et Technique du Bâtiment	UNIGE	University of Geneva
		ZAMG	Zentralanstalt für Meteorologie und Geophysik/Geodynamik

Table I List of the stations, data and parameters availability.

and Eppley PSP pyranometers, and Eppley NIP pyrheliometers, are used to acquire the data. A stringent calibration, characterization and quality control was applied on all the data by the person in charge of the measurements, the coherence of the data for all the stations was verified by the author and is described in the following section. For two sites, the aerosol optical depth aod and the water vapor column w is independently acquired and is used as input to clear sky models in order to assess the instruments calibration factors.

The climate, latitude, longitude and altitude of the stations are given in Table I.

3. Data quality control

For all the stations, the first quality control consist of an assessment of the acquisition time stamp. To point out a possible time shift in the data, the symmetry in solar time of the irradiance for very clear days is visually checked. The horizontal global and if available, the normal beam irradiances are plotted versus the sinus of the solar elevation angle for specific clear days. If the time stamp is correct, the afternoon curve should lay over the morning curve as visualized on Figure 1a.

If this test is positive, a verification can be done with the help of the global clearness index K_t defined as:

$$K_t = \frac{G_h}{I_o \cdot \sin(h)}$$

where G_h is the horizontal global irradiance, I_o is the solar constant, and h the solar elevation angle. The clearness index is plotted for the morning and the afternoon data in a separate color. The upper limit, representative of clear sky conditions, should lay

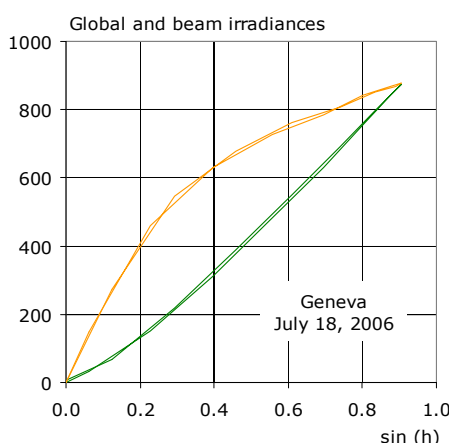


Figure 1a The global horizontal and normal beam irradiances are represented versus the sinus of the solar elevation angle for a clear day.

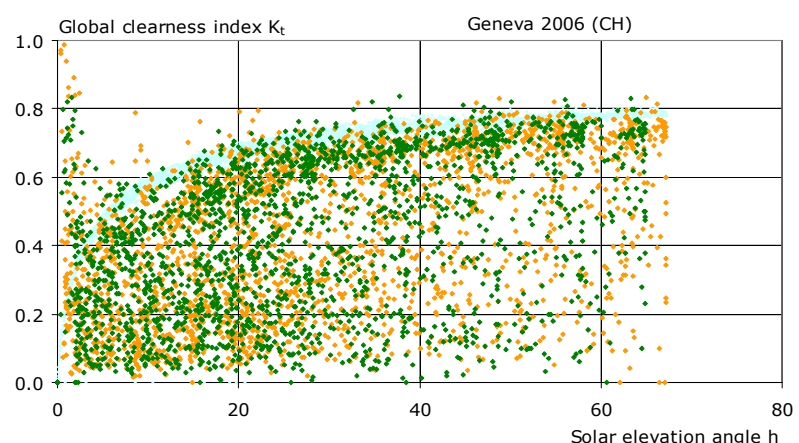


Figure 1b The global clearness index K_t is represented separately for the morning (green) and the afternoon (yellow) data, versus the solar elevation angle for one year in hourly values. Clear sky model data are represented in blue.

over for the morning and the afternoon data as represented on Figure 1b for one year of data acquired at the site of Geneva for the year 2006. Hourly clear sky condition values are plotted in light blue on the same graph. When these two conditions are fulfilled, the time stamp of the data bank is correct, and the solar geometry can be precisely calculated. This test is very sensitive and a time shift of only a few minutes will conduct to an visible assymetry. A similar test can be done with the beam clearness index K_b defined as:

$$K_b = \frac{B_n}{I_o}$$

but this parameter is less sensitive to a possible time shift.

The coherence test between the two components can be verified with the help of the global and beam clearness indices (Ineichen 2010). The hourly beam clearness index is plotted versus the corresponding global index as illustrated on Figure 2 for the site of Carpentras. On the same graph, the clear sky data evaluated with the Solis clear sky model (Müller 2004, Ineichen 2008a) are represented for four different values of aerosol optical depth (aod). The more usual corresponding Linke turbidity coefficient T_{Lam2} retrieved from the beam irradiance:

$$B_n = I_o e^{(-\delta_{cda} \cdot T_{Lam2} \cdot MA)}$$

and evaluated at air mass $AM = 2$ is also given on the graph (Linke 1922, Ineichen 2008b). δ_{cda} is the optical depth of a clean and dry atmosphere. An important deviation from the clear sky lines can indicate calibration uncertainties, beam irradiance missalignement or soiled sensors.

The absolute sensor calibration can be assessed with the help of a clear sky model when the atmospheric aerosol optical depth and the water vapor column are known. These two parameters are normally retrieved from spectral measurements. When the

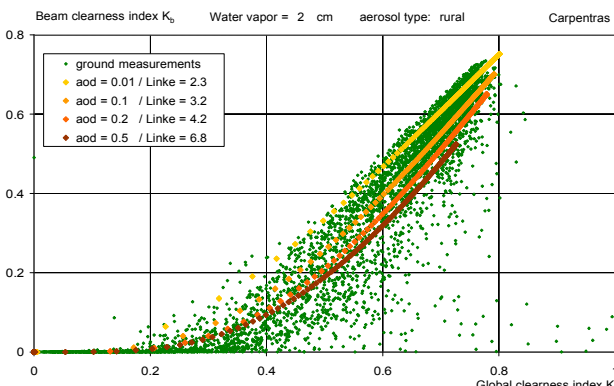


Figure 2 The beam clearness index is plotted against the global clearness index. On the same graph, clear sky modelled values are represented for 4 different aerosol loads

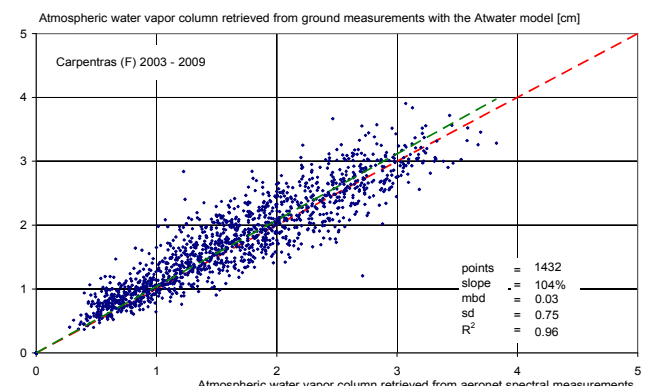


Figure 3 Atmospheric water vapor column evaluated from the ambient temperature and relative humidity against the watre vapor retrieved from spectral measurements.

water vapor w is missing, it can be evaluated from the ground ambient temperature (T_a) and relative humidity (HR) by the use of Atwater model (Atwater 1976) with a good precision as illustrated on Figure 3 for the site of Carpentras and data acquired from 2003 to 2009.

For some sites, the aod measurements retrieved from independent networks such as aeronet are acquired as soon as direct sun is available; these values are then averaged to give a daily value and used with the Solis clear sky model to evaluate hourly clear sky G_h and B_n values.

Day by day, the highest hourly value is then selected from the measurements and plotted against the day of the year on Figure 4. These points are representative of the clearest daily sky conditions. Based on the aod and water vapor content w of the atmosphere, the corresponding clear sky values are evaluated with the model. As the highest values for each day is selected, the upper limit for these two series should lay together if the two sets of measurements (irradiance and aod) are coherent. On the same graph are also represented the daily clear sky indices defined as:

$$K_h = \frac{\sum_{day} G_h}{\sum_{day} G_{hc}} \quad \text{and} \quad K_{hb} = \frac{\sum_{day} B_n}{\sum_{day} B_{nc}}$$

These values, if the data are coherent, should have an upper limit near of the unity.

4. The clearness index K_t and sky type classification

As it is the case for the majority of the national networks, the global irradiance is the only available measured parameter concerning the solar radiation. Even if for half of the stations the beam component is available, the global irradiance and the corresponding

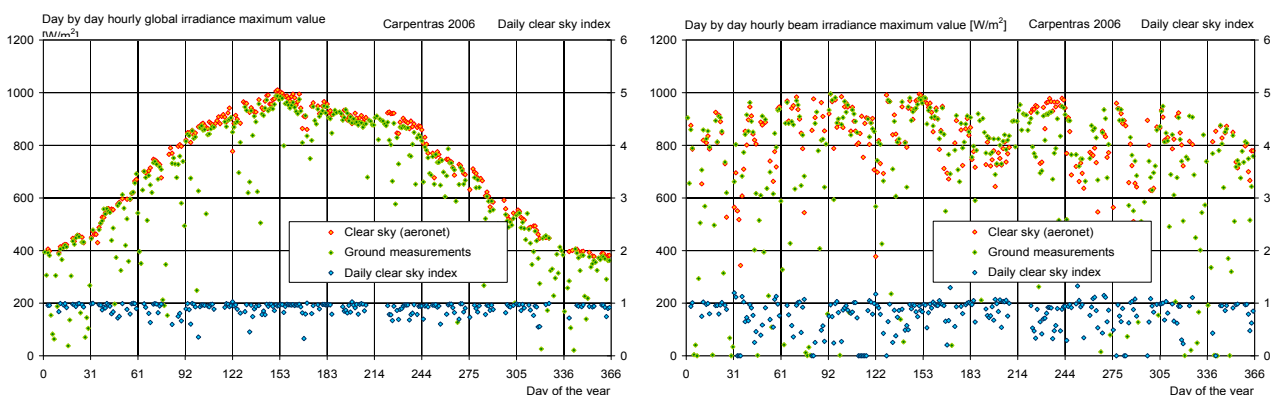


Figure 4 Daily highest value of the global irradiance reported versus the day of the year for the station of Carpentras, for the measurements and the corresponding clear sky evaluated from the aod and the Solis model. The daily clear sky index is also represented.

clearness index K_t are key parameters in the field of irradiance modelization. The clearness index K_t was introduced as a norm (Black 1954) to characterize the insulation conditions at a given point in time when only the global component is known. Unfortunately, this parameter is not independent of the solar elevation angle as it is shown on the left graph of Figure 5 where the clearness index K_t is plotted versus the solar elevation angle for the site of Carpentras. It can be seen on this Figure that clear sky conditions, determined by the upper limit of the clearness index values, are not equally represented by K_t for the different solar elevation angles.

In order to use the clearness index as a reliable sky condition descriptor, Perez et al. (1990) modified this parameter to make it independent of the solar elevation angle. The formulation is the following:

$$K'_t = \frac{K_t}{(1.031 \cdot \exp(-1.4 / (0.9 + 9.4 / AM)) + 0.1)}$$

where AM is the optical air mass as defined by Kasten (1980). This modified clearness index is represented on Figure 5 (right graph) for the same points than above. It can clearly be seen on this Figure that even if some patterns are still present, the modified clearness index is relatively independent from the solar elevation angle. Therefore, it is now possible to define three zones to characterize three sky types:

clear sky conditions	$0.65 < K'_t \leq 1.00$
intermediate sky conditions	$0.30 < K'_t \leq 0.65$
cloudy sky conditions	$0.00 < K'_t \leq 0.30$

These limits are arbitrary, but are coherent with other classifications, like for example the Cloud Free Index saturation ($CFIsat$) as defined by Dürr (2006):

$$CFIsat = 100 (CFI - 1) / z$$

where z and CFI are defined in Dürr (2004). $CFIsat$ is independent from the irradiance measurements; it is a function of the downward surface longwave irradiance and the dry bulb temperature. The comparison between the $CFIsat$ and K'_t is illustrated on Figure 6 (right graph). The red dashed lines represent the limits used in the present study and applied on the modified clearness index. In the $CFIsat$ classification, clear sky conditions are defined by a $CFIsat$ below 0%, and cloudy conditions above 50%. The corresponding limits are represented in blue dashed lines. It can be seen on Figure 6 that the majority of the points are situated in the intersections of the corresponding three zones.

Another assessment can be done with the cloud cover as illustrated on Figure 6 (left graph). Here also, the limits used in the present study are well correlated with the cloud

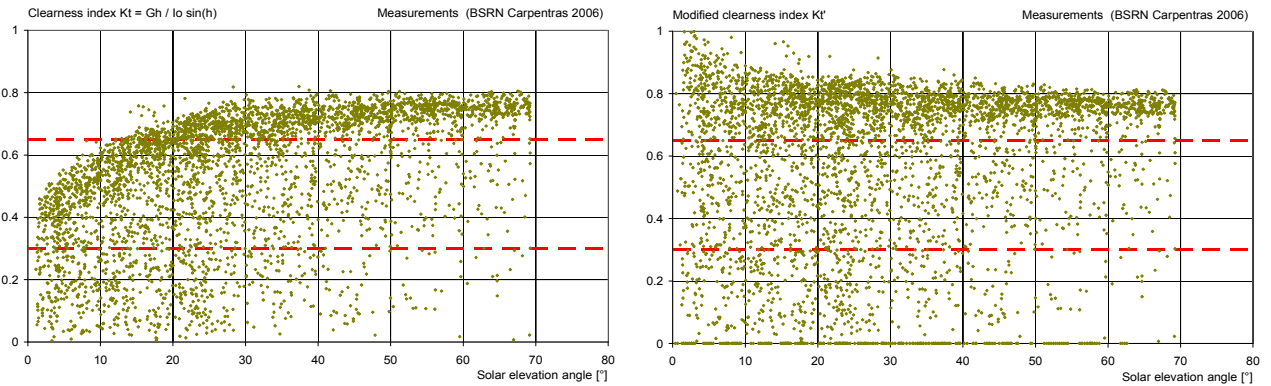


Figure 5 Global and modified clearness index versus the solar elevation angle.

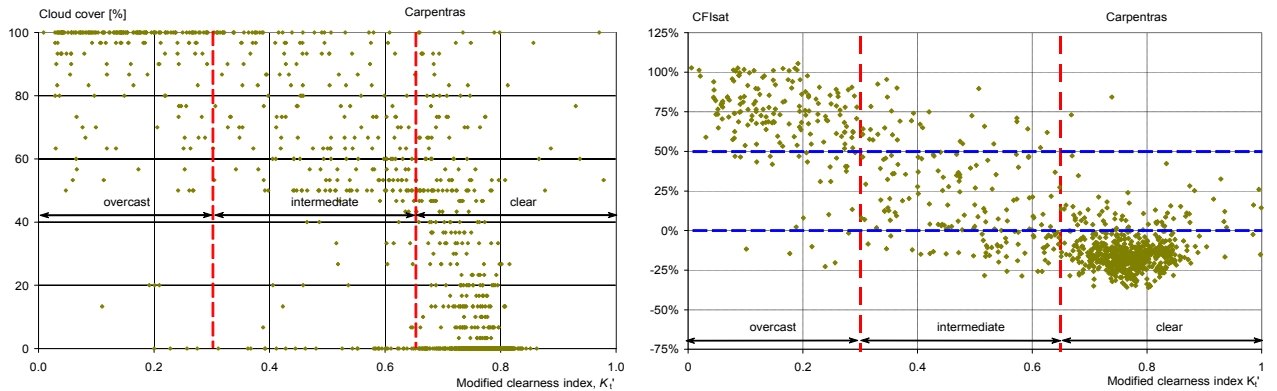


Figure 6 Cloud cover and *CFIsat* coefficient versus the modified clearness index. The sky condition selection limits are represented in dashed red lines.

cover (0% cloud cover for the clear sky conditions and 100% cloud cover for the overcast sky conditions).

5. Satellite derived data

Five different products are validated in the present study. The methodology and the input parameters are described in the following section. The product from University of Oldenburg (EnMetSol) is evaluated for two different aerosol climatologies.

5.1 SolarGis

The irradiance components are the results of a five steps process: a multi-spectral analysis classifies the pixels, the lower boundary (LB) evaluation is done for each time slot, a spatial variability is introduced for the upper boundary (UP) and the cloud index definition, the Solis clear sky model is used as normalization, and a terrain disaggregation is finally applied.

Four MSG spectral channels are used in a classification scheme to distinguish clouds from snow and no-snow cloud-free situations. Prior to the classification, calibrated pixel values were transformed to three indices: normalized difference snow index (Ruyter 2007), cloud index (Derrien 2005), and temporal variability index. Exploiting the potential

of MSG spectral data for snow classification removed the need of additional ancillary snow data and allowed using spectral cloud index information in cases of complex conditions such as clouds over high albedo snow areas.

In the original approach by Perez (2002), the identification of surface pseudo-albedo is based on the use of a lower bound (LB), representing cloudless situations. This approach neglects diurnal variability of LB that is later corrected by statistical approach. Instead of identifying one value per day, LB is represented by smooth 2- dimensional surface (in day and time slot dimensions) that reflects diurnal and seasonal changes in LB and reduces probability of no cloudless situation.

Overcast conditions represented in the original Perez model by a fixed Upper Bound (UB) value were updated to account for spatial variability which is important especially in the higher latitudes. Calculation of cloud index was extended by incorporation of snow classification results.

The broadband simplified version of Solis model (Ineichen 2008a) was implemented. As input of this model, the climatology values from the NVAP water vapor database (Randl 1996) and Atmospheric Optical Depth data by (Remund 2008) assimilated with Aeronet and Aerocom datasets are used.

Simplified Solis model was also implemented into the global to beam Dirindex algorithms to calculate Direct Normal Irradiance component (Perez 1992, Ineichen 2008c). Diffuse irradiance for inclined surfaces is calculated by updated Perez model (1987).

Processing chain of the model includes post-processing terrain disaggregation algorithm based on the approach by Ruiz-Arias (2010). The disaggregation is limited to shadowing effect only, as it represents most significant local effect of terrain. The algorithm uses local terrain horizon information with spatial resolution of 100 m. Direct and circumsolar diffuse components of global irradiance were corrected for terrain shadowing.

5.2 Heliosat-2 algorithm

The Helioclim 3 data bank is produced with the Heliosat-2 method that converts observations made by geostationary meteorological satellites into estimates of the global irradiation at ground level. This version integrates the knowledge gained by various exploitations of the original Heliosat method and its varieties in a coherent and thorough way.

It is based upon the same physical principles but the inputs to the method are calibrated radiances, instead of the digital counts output from the sensor. This change opens the possibilities of using known models of the physical processes in atmospheric optics, thus removing the need for empirically defined parameters and of pyranometric measurements to tune them. The ESRA models (ESRA 2000, Rigollier 2000 and 2004) are used for modeling the clear-sky irradiation. The assessment of the ground albedo

and the cloud albedo is based upon explicit formulations of the path radiance and the transmittance of the atmosphere. The turbidity is based on climatic monthly Linke Turbidity coefficients data banks.

The Liu and Jordan (1960) model is used to split the global irradiance into the diffuse and beam components.

5.3 3Tier algorithm

Satellite-based time series of reflected sunlight are used to determine a cloud index time series for every land surface worldwide. A satellite based daily snow cover dataset is used to aid in distinguishing snow from clouds. In addition, the global horizontal clearsky radiation G_{hc} is modeled based on the surface elevation of each location, the local time, and the measure of turbidity in the atmosphere. 3Tier opted to use a satellite-based, monthly time series of aerosol optical depth and water vapor derived from the Moderate Resolution Imaging Spectroradiometer (MODIS). This dataset was combined with another turbidity dataset that includes both surface and satellite observations to provide a turbidity measure that spans the period of our satellite dataset and is complete for all land surfaces. The cloud index n and the clear sky irradiance G_{hc} are then combined to model the global horizontal irradiance G_h . This component of the process is calibrated for each satellite based on a set of high-quality surface observations. G_h estimates are then combined with other inputs to evaluate the other irradiance components D_h and B_n .

5.4 EnMetSol

The EnMetSol method is a technique for determining the global radiation at ground by the use of data from a geostationary satellite (Beyer 1996, Hammer 2003). It is used in combination with a clear sky model to evaluate the 3 irradiance parameters G_h , D_h and B_n . The key parameter of the method is the cloud index n , which is estimated from the satellite measurements and related to the transmissivity of the atmosphere via

$$K_c = 1 - n$$

where the transmissivity is expressed by the clear sky index K_c defined as the ratio of global irradiance G_h and the corresponding clear sky irradiance G_{hc} :

$$K_c = \frac{G_h}{G_{hc}}$$

Two sets of data produced with the EnMetSol algorithm will be analyzed, corresponding to two different clear sky irradiance models:

- the model of Dumortier (Fontoynon 1998) with the Remund (2009) MeteonormHR high resolution data base for the turbidity input,

- and the original Solis clear sky model (Mueller 2004) with monthly averages of AOD (Kinne 2005) and water vapour content (Kalnay 1996) as input parameters.

For the Dumortier clearsky, a diffuse fraction model (Lorenz 2007) is used to calculate the all sky diffuse horizontal irradiance (via G_h - D_h). A recently developed beam fraction model (Hammer 2009) is used to calculate the B_n for all sky conditions with the Solis model.

5.5 IrSolAv

In the IrSolAv irradiance derivation scheme, the cloud index n is derived using the methodology developped by Dagestad and Olseth (Dagestad and Olseth, 2007) with some modifications in the ground albedo determination. The ground albedo is computed from a forward and backward moving window of 14 days taking into account its evolution during the day, as function of the co-scattering angle.

The global horizontal irradiance G_h is then evaluated from the cloud index with the model proposed by Zarzalejo (Zarzalejo et al., 2009); it uses as independent variables the cloud index, the 50-percentile of the cloud index for a given place, and the air mass AM . The normal beam irradiance B_n is calculated from the global irradiance with the help of Louche correlation (Louche et al., 1991).

In a second step, the clear sky conditions are indentified with the algorithm proposed by Polo (Polo et al., 2009a; Polo et al., 2009b); for these clear conditions, the irradiances are evaluated with the ESRA clear sky model (Rigollier 2000), using the aerosol optical depth aod taken from Soda, MODIS or from a method proposed by Polo (Polo et al., 2009a) depending on their availability.

6. Comparison and evaluation procedure

In terms of validation, when evaluating satellite derived parameters with the same time

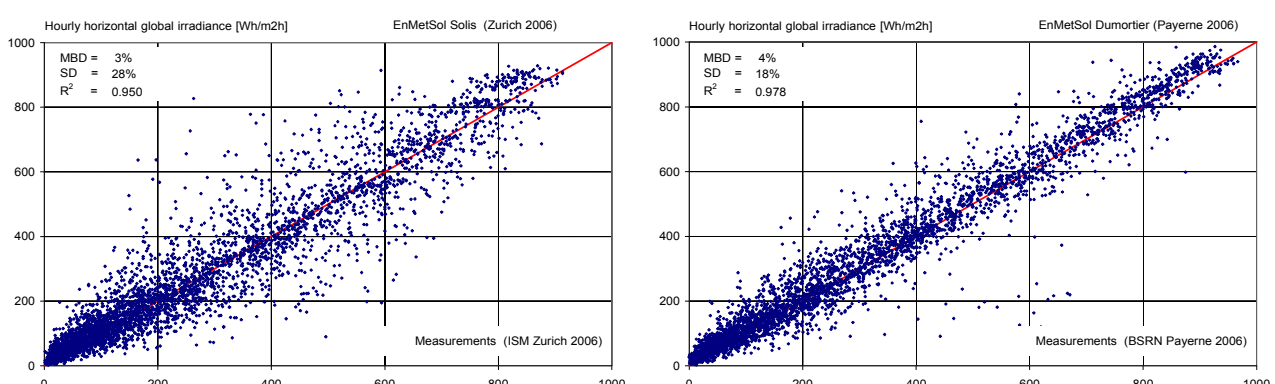


Figure 8 Scatter plots for the global horizontal irradiance produced by EnMetSol for Zurich and Payerne.

step, the comparison can be done by means of scatter plots; these give a visual evaluation of the capability of the model to reproduce the measurements. On these graphs, the diagonal line is representative of an ideal model, and the points should lay around this line. An illustration is given on Figure 8 for Zurich and Payerne, two sites that showing different dispersions.

The statistical parameters like the mean bias difference (*mbd*), the root mean square difference (*rmsd*), the standard deviation (*sd*) and the determination coefficient (R^2) represent a quantification of the model dispersion. These statistical parameters include dispersions introduced by:

- the retrieval procedure,
- the comparison of point measurements (ground data) with aera measurements,
- the comparison of the average of four instantaneous measurements with 60 minutes integrated values.

In the field of solar radiation and natural light, the comparison is often done in term of frequency of occurrence: for the irradiance, it gives an indication of the repartition for each level of radiation, and for the clearness index, that the level of radiation occurs at the right time during the day. The obtained graph is a line (or a bar chart) representative of the relative frequency of occurrence of the considered parameter. This is illustrated on Figure 9 for the global irradiance and the corresponding clearness index K_t . On the same graph, the frequency of occurrence of the ground measurements are represented as grey bars, and the different models in color lines.

A second order statistic, the Kolmogorov-Smirnov test (Espinar 2009), is also applied to the data. It represents the capability of the model to reproduce the frequency of occurrence at each of the irradiance level. In order to avoid a peak at the zero level of beam irradiance, these values are excluded form the statistic. A visualisation is given on Figure 10 where the irradiance cumulated frequency of occurrence is represented against

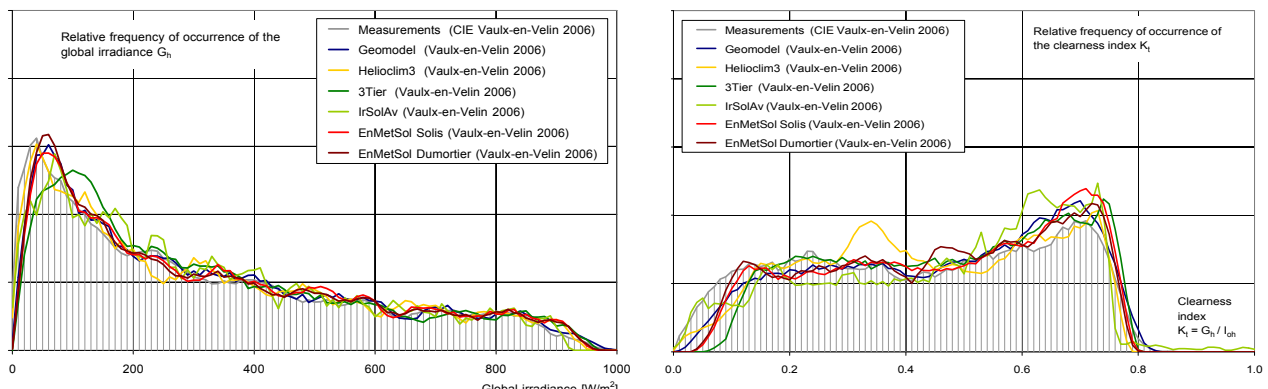


Figure 9 Global irradiance and clearness index K_t relative frequency of occurrence for data acquired in Vaulx-en-Velin (F). The grey bars are representative of the measurements.

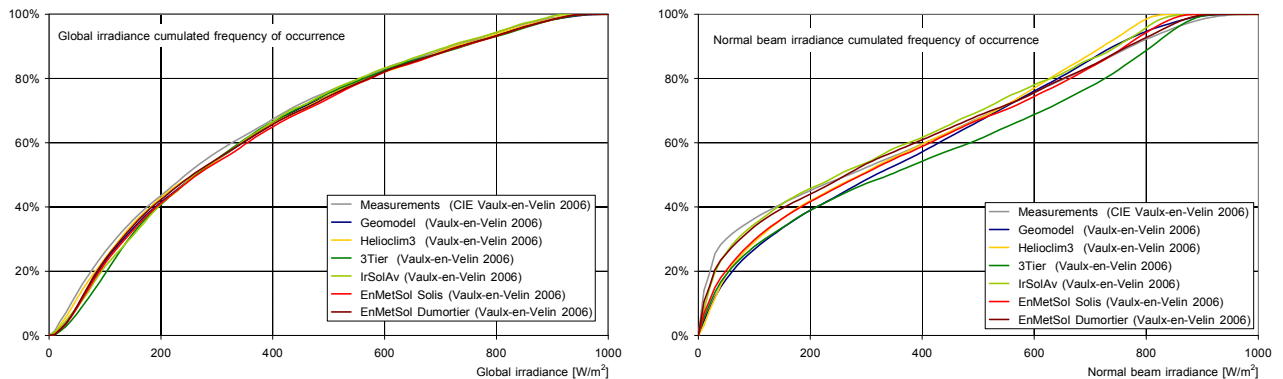


Figure 10 Relative frequency of occurrence for the global and the beam irradiance for measurements at the site of Vaulx-en-Velin.

the irradiance for the same site than above. The quantitative value representative of the Kolmogorov Smirnov test Integral (*KSI*) is defined as:

$$KSI = \int_{G_{h\min}}^{G_{h\max}} |F_c(G_h) - F_c(G_{h\text{mod}})| \cdot dG_h$$

where $F_c(G_h)$ and $F_c(G_{h\text{mod}})$ are respectively the ground measurements and the corresponding modelled cumulated frequencies of occurrence.

7. Global irradiance results

To ensure a correct and comparable validation of the different products, the following method was used to merge the products and the ground measurements: for each generated value, the nearest time stamped corresponding ground value is searched in the data base; this means that the satellite image was taken within the ground integration

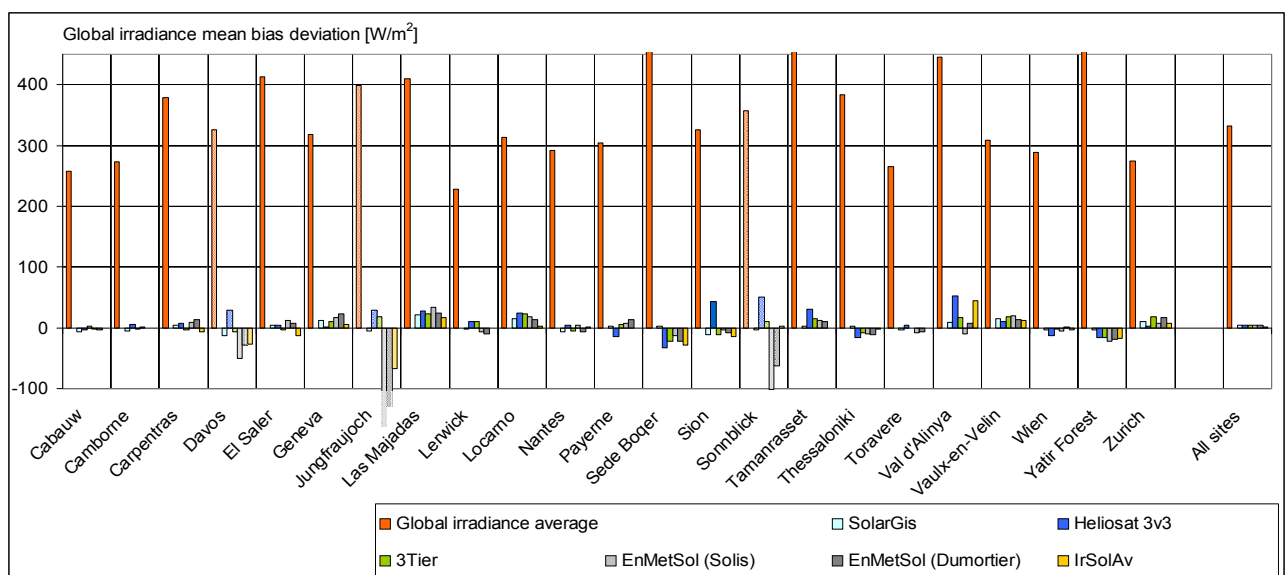


Figure 11 Average global irradiance and absolute mean bias difference

	G_h [W/m ²]	nb	R ²	SolarGIS			R ²	Heliosat 3v3			R ²	3Tier			R ²	EmMetSol (Solis)			R ²	EmMetSol (Dumortier)			R ²	IrSolAv			sd	KSI
				mbd	sd	KSI		mbd	sd	KSI		mbd	sd	KSI		mbd	sd	KSI		mbd	sd	KSI		mbd	sd	KSI		
Cabauw	258	4153	0.977	-6	49	9	0.967	-4	58	5	0.961	3	63	16	0.982	-1	43	6	0.981	-3	44	8	0.901	-6	121	11		
Camborne	273	4087	0.976	-6	52	8	0.966	6	63	9	0.981	-2	66	15	0.981	1	47	8	0.981	0	47	8	0.934	-28	147	34		
Carpentras	379	3993	0.985	4	48	4	0.978	7	59	10	0.980	-4	55	9	0.987	8	45	9	0.996	14	46	14	0.962	-13	75	19		
Davos	326	4200	0.942	-13	89	19	0.915	29	107	31	0.915	-6	107	21	0.946	-50	51	9	0.937	-29	92	33	0.934	-28	147	34		
El Saler	413	3600	0.971	4	67	6	0.971	3	67	9	0.959	-3	78	11	0.976	12	60	12	0.976	7	60	8	0.962	-13	75	19		
Geneva	317	3622	0.977	12	55	12	0.974	1	59	4	0.960	10	72	12	0.983	16	47	11	0.982	22	50	22	0.943	5	86	11		
Jungfraujoch	399	3311	0.899	-4	132	8	0.817	29	170	49	0.811	18	177	25	0.703	-161	208	162	0.697	-130	210	131	0.689	-67	217	67		
Las Majadas	410	3509	0.978	21	62	21	0.970	28	68	28	0.966	23	73	23	0.978	34	58	34	0.979	24	57	24	0.963	16	75	16		
Lerwick	228	3306	0.958	-2	59	10	0.930	11	78	18	0.920	10	80	18	0.964	-7	54	13	0.964	-10	54	14	0.955	2	79	19		
Locarno	314	4184	0.979	16	54	15	0.955	24	80	24	0.959	23	75	23	0.981	19	51	19	0.979	14	54	14	0.943	1	81	9		
Nantes	232	4200	0.979	-7	49	9	0.948	4	79	14	0.963	-5	65	14	0.984	4	44	7	0.983	-7	45	10	0.943	-1	85	16		
Payerne	304	4005	0.976	3	57	4	0.964	-14	68	14	0.958	5	74	11	0.978	8	53	8	0.978	14	55	13	0.943	-1	85	16		
Sede Boquer	576	2890	0.986	1	51	11	0.982	-34	57	33	0.970	-24	73	27	0.985	-15	53	18	0.986	-23	53	25	0.974	-29	70	32		
Sion	325	4280	0.963	-11	75	21	0.947	43	88	43	0.954	-11	83	26	0.978	-8	61	17	0.986	-14	126	33	0.975	-8	172	17		
Sonnblick	357	3933	0.858	-3	134	16	0.838	50	143	50	0.806	11	159	24	0.757	-102	159	102	0.747	-63	168	64	0.765	2	172	17		
Tamansasset	529	4293	0.985	3	56	5	0.988	30	85	30	0.970	15	80	15	0.970	11	78	14	0.972	10	76	15	0.959	-2	80	15		
Thessaloniki	384	3675	0.982	3	53	3	0.978	-16	60	16	0.964	-8	76	16	0.975	-9	63	14	0.975	-11	64	16	0.959	-2	80	15		
Torrevieja	266	3784	0.971	-4	53	4	0.940	3	80	16	0.944	-1	72	21	0.973	-8	51	10	0.972	-7	52	9	0.927	-17	52	9		
Val d'Alanya	446	2499	0.968	9	73	11	0.927	52	117	52	0.951	17	94	17	0.965	-10	80	23	0.966	7	78	17	0.927	45	116	45		
Vaulx-en-Velin	308	4141	0.980	15	51	14	0.972	11	60	11	0.965	18	66	18	0.983	19	46	19	0.983	14	47	14	0.950	11	79	13		
Wien	288	4203	0.973	-3	55	6	0.969	-13	61	13	0.963	-2	64	13	0.981	-5	47	7	0.981	1	47	3	0.932	-3	87	11		
Yair Forest	549	3221	0.984	-4	53	7	0.980	-16	59	18	0.974	-16	66	17	0.988	-22	47	23	0.987	-20	47	21	0.972	-18	69	18		
Zurich	274	4192	0.953	10	74	12	0.940	3	87	13	0.937	18	85	19	0.950	8	76	9	0.950	16	79	16	0.920	7	95	10		
All sites	332	75837	n/a	3	55	n/a	n/a	4	70	n/a	n/a	4	70	n/a	n/a	4	54	n/a	n/a	4	55	n/a	n/a	1	83	n/a	n/a	

Table II First and second order statistics in absolute values for the global horizontal irradiance. The sites in grey are not taken into account in the overall statistics.

	G_h [W/m ²]	nb	R ²	SolarGIS			R ²	Heliosat 3v3			R ²	3Tier			R ²	EmMetSol (Solis)			R ²	EmMetSol (Dumortier)			R ²	IrSolAv			sd%	KSI
				mbd%	sd%	KSI		mbd%	sd%	KSI		mbd%	sd%	KSI		mbd%	sd%	KSI		mbd%	sd%	KSI		mbd%	sd%	KSI		
Cabauw	258	4153	0.977	-3	19	9	0.967	-2	23	5	0.961	-1	24	16	0.982	-1	17	6	0.981	0	17	8	0.901	-2	32	11		
Camborne	273	4087	0.976	-2	13	4	0.966	2	16	10	0.980	-1	14	9	0.987	2	12	9	0.986	4	12	14	0.901	-2	32	11		
Carpentras	379	3993	0.985	1	27	19	0.978	2	33	31	0.915	-2	33	21	0.946	-15	27	51	0.937	-9	28	33	0.834	-8	45	34		
Davos	326	4200	0.942	-4	11	5	0.971	1	16	9	0.959	-1	19	11	0.976	3	14	12	0.976	2	14	8	0.962	-3	18	19		
El Saler	413	3600	0.971	-4	17	12	0.974	0	19	4	0.960	3	23	12	0.983	5	15	11	0.982	2	16	8	0.943	0	27	11		
Geneva	317	3622	0.977	-1	33	8	0.899	7	43	49	0.811	5	44	25	0.703	-40	52	162	0.697	-33	53	131	0.689	-17	54	67		
Jungfraujoch	399	3311	0.976	5	21	10	0.970	7	17	28	0.966	6	18	23	0.978	8	14	34	0.979	6	14	24	0.963	4	18	16		
Las Majadas	410	3509	0.958	-1	26	15	0.930	5	34	18	0.920	4	35	18	0.964	-3	24	13	0.964	-4	24	14	0.955	1	25	19		
Lerwick	228	3306	0.958	5	17	15	0.965	8	25	24	0.959	7	24	23	0.981	6	16	19	0.979	4	17	14	0.943	0	28	9		
Locarno	314	4184	0.979	-2	17	9	0.948	1	27	6	0.963	-2	22	14	0.984	1	15	7	0.983	-2	16	10	0.943	0	28	9		
Nantes	232	4200	0.976	1	19	4	0.964	-5	23	14	0.958	2	24	11	0.978	3	17	8	0.978	4	18	13	0.943	0	28	16		
Payerne	304	4005	0.976	0	9	11	0.982	-6	10	33	0.970	-4	13	27	0.985	-3	9	18	0.986	4	9	25	0.974	-5	12	32		
Sede Boquer	576	2890	0.986	-3	23	21	0.947	13	27	43	0.954	-3	26	26	0.978	-1	18	16	0.986	-4	19	17	0.886	-4	39	33		
Sion	325	4280	0.963	-1	38	16	0.838	14	40	50	0.806	3	44	24	0.757	-29	45	102	0.747	-18	47	64	0.765	1	48	17		
Sonnblick	357	3933	0.858	-1	0	11	5	0.968	6	16	10	0.970	3	15	15	0.970	2	15	14	0.972	2	14	15	0.959	-1	21	15	
Tamansasset	529	4293	0.985	1	14	3	0.978	-4	16	16	0.964	-2	16	20	0.975	-2	16	14	0.975	-3	17	16	0.959	-1	21	15		
Thessaloniki	384	3675	0.982	-1	20	4	0.940	1	30	16	0.944	0	27	21	0.973	-3	19	10	0.972	-3	20	9	0.927	10	26	45		
Torrevieja</td																												

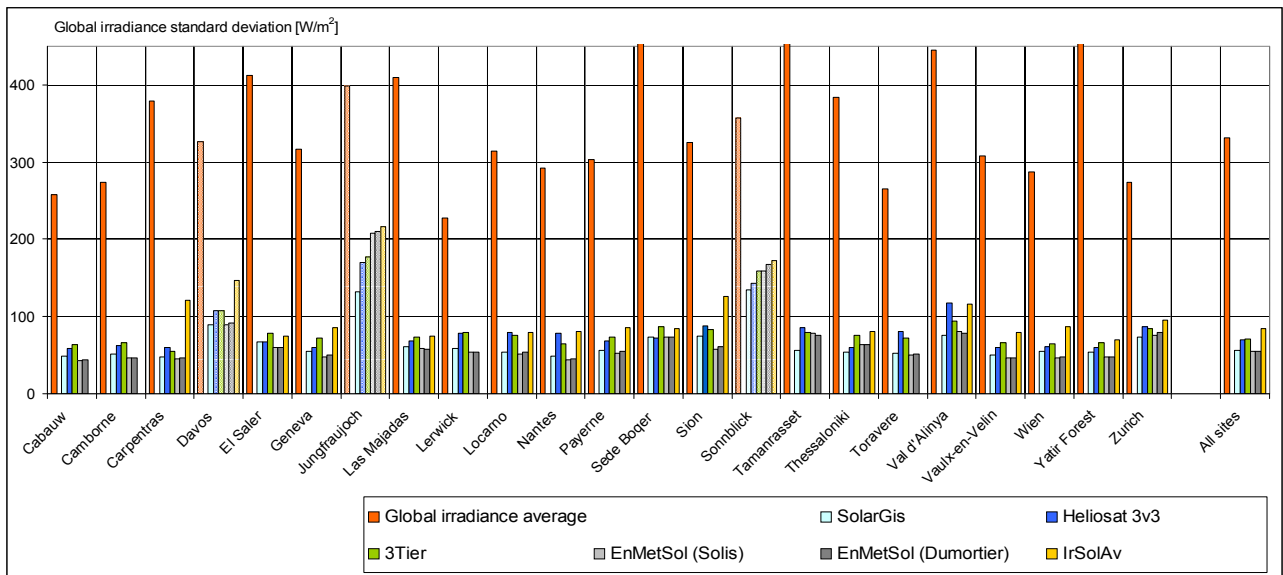


Figure 12 Absolute standard deviation for the global irradiance. In red, the average G_h .

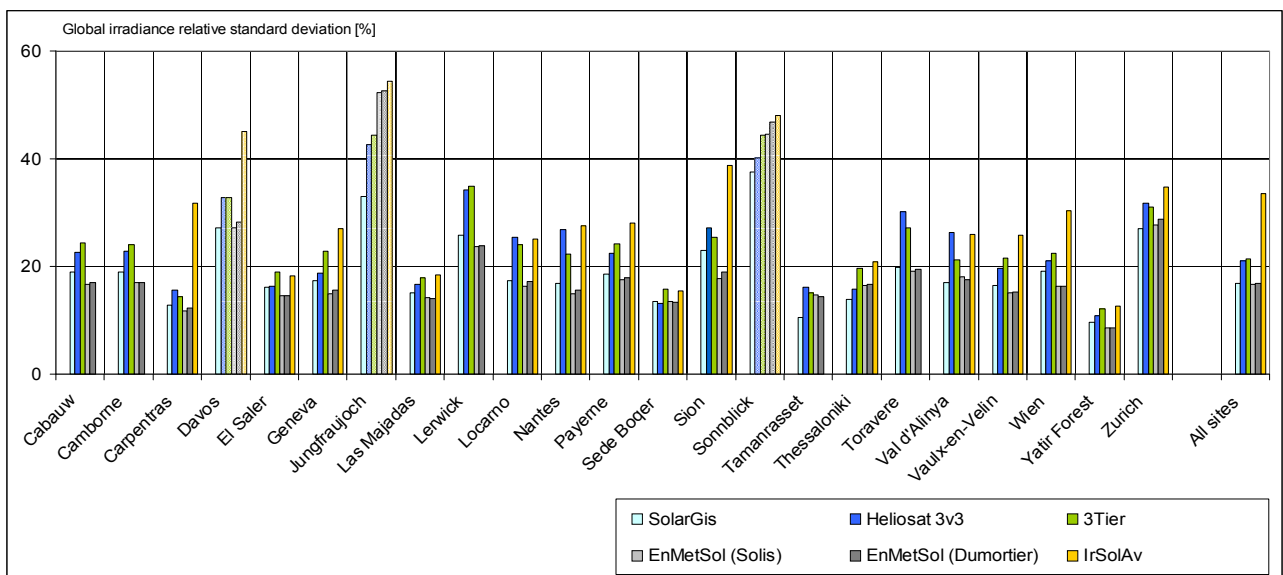


Figure 13 Relative standard deviation for the global irradiance.

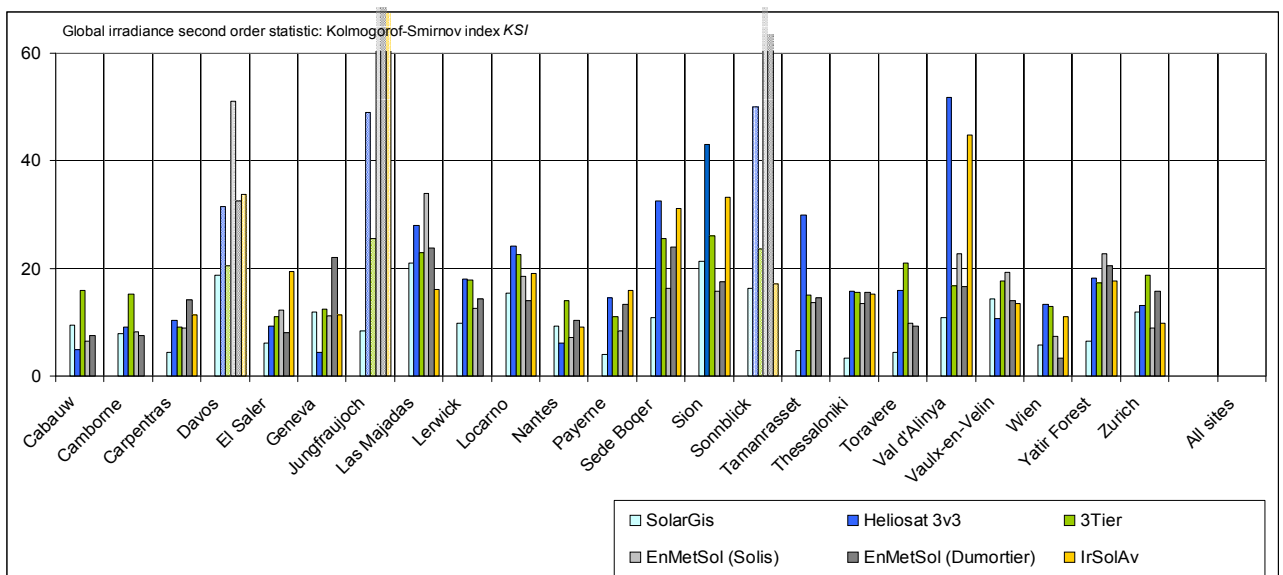


Figure 14 Second order statistics KSI for the global irradiance

period. Then, only hours for which ground and both generated products are present are taken into account in the validation procedure; so, mainly the ground data availability restrict the number of points in the comparison.

The results of the validation are given on Table II and Table III respectively in absolute and relative values. The corresponding graphs are given on Figure 11 to 14.

The first established fact is that the sites of Davos, Jungfraujoch and Sonnblick give much higher differences than the other stations. This is due to the snow cover during all or part of the year, which is not taken into account by all the models, and is difficult to evaluate precisely. This is clearly visible on frequency of occurrence plotted for the clearness index as shown on Figure 15 for the site of Sonnblick. These site are not part of the overall statistics. The site of Nantes is also represented on Figure 15 for comparison purpose.

The overall average mean bias deviation is very low for all the products, and except for heliosat 3, the sign of the mean bias deviation is in general the same for all the algorithms. It is interesting to note that for high latitude sites (Cabauw, Camborne, Lerwick and Toravere), the bias is even lower than for the middle latitude sites. The site of Val d'Alynia in Spain shows slightly variable bias depending on the product, this can be explained by

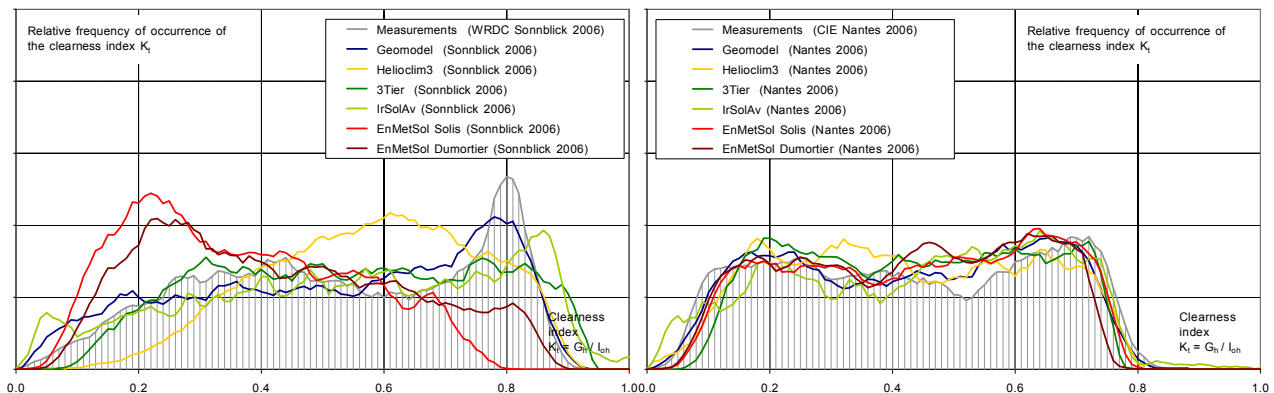


Figure 15 Frequency of occurrence of the clearness index for the site of Sonneblick (high altitude and snow) and for Nantes.

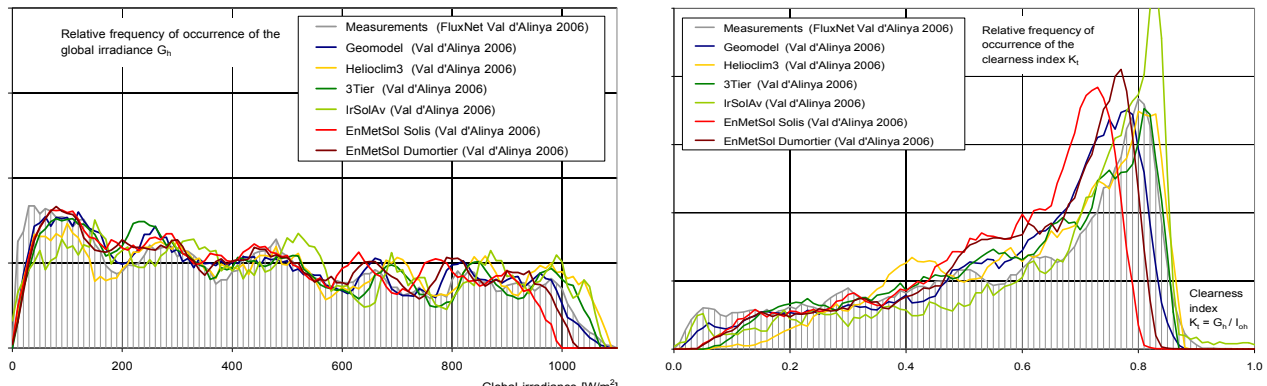


Figure 16 Frequency of occurrence of global irradiance and the clearness index for the site of Val d'Alynia.

the high altitude of the site (1770m) and the mountainous environment. The produced irradiance varie from one algorithm to the other; the corresponding graph is given on Figure 16 for the global irradiance and the clearness index. This can be due to the clear sky model used for the normalisation in conjunction with their input parameter (atmospheric water vapor content, aerosol load and linke turbidity).

In term of absolute standard deviation (due to the negligible bias, the root mean square difference and the standard deviation are equivalent), except for the high altitude stations (Davos, Jungfraujoch, Sonnblick and Val d'Alynia), all the site show the same order of magnitude, including the high latitude sites. Due to the high irradiance level for Carpentras, Sede Boquer, Tamanrasset and Yatir forest, the sites show good relative standard deviations.

The choice of a clear sky model is a key point in the satellite irradiance derivation, it will have a direct influence on the output. The measured and modelled global clearness

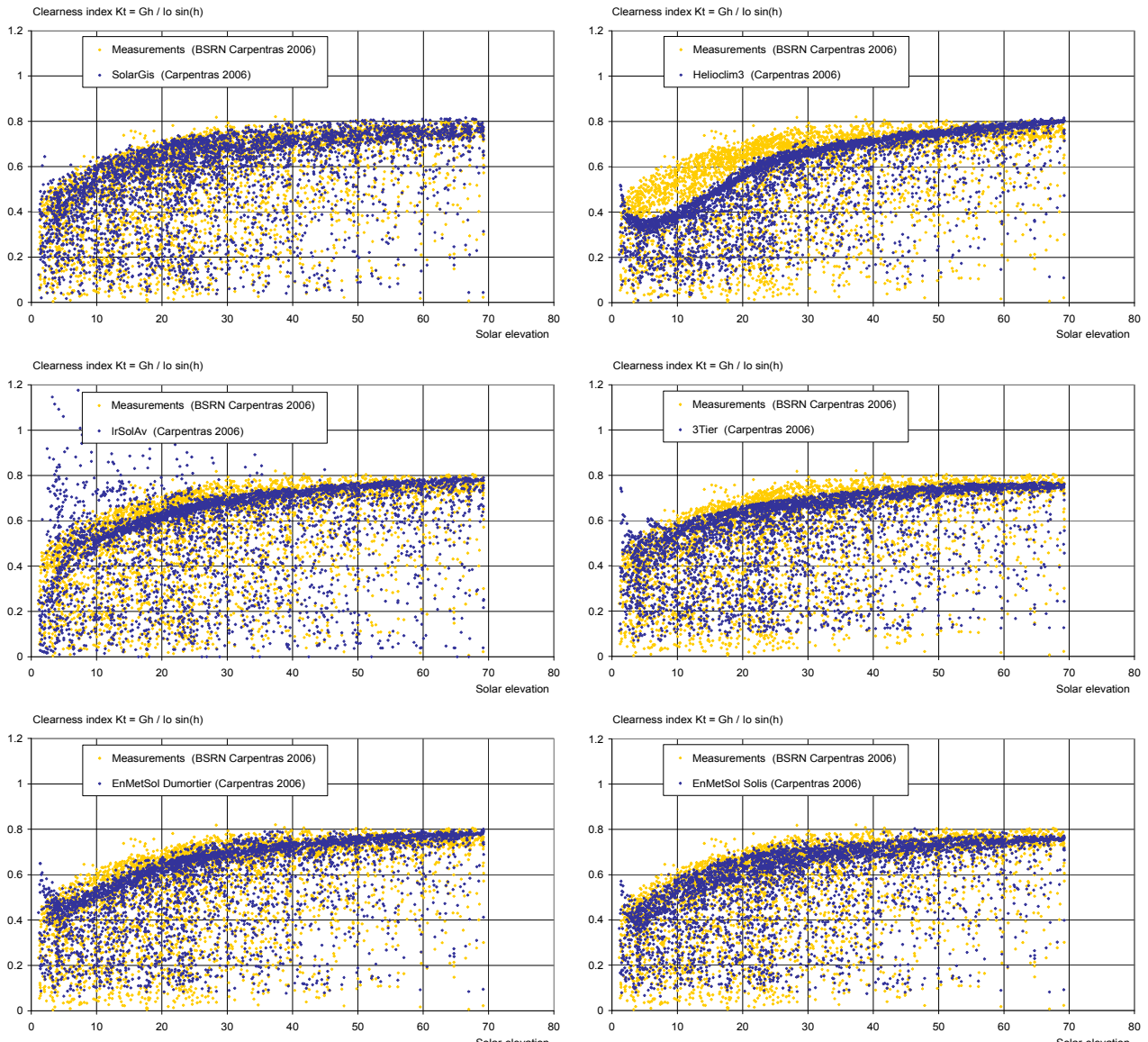


Figure 17 The global clearness index K_t represented against the solar elevation angle for the site of Carpentras. In yellow, the measurements and in blue the different products.

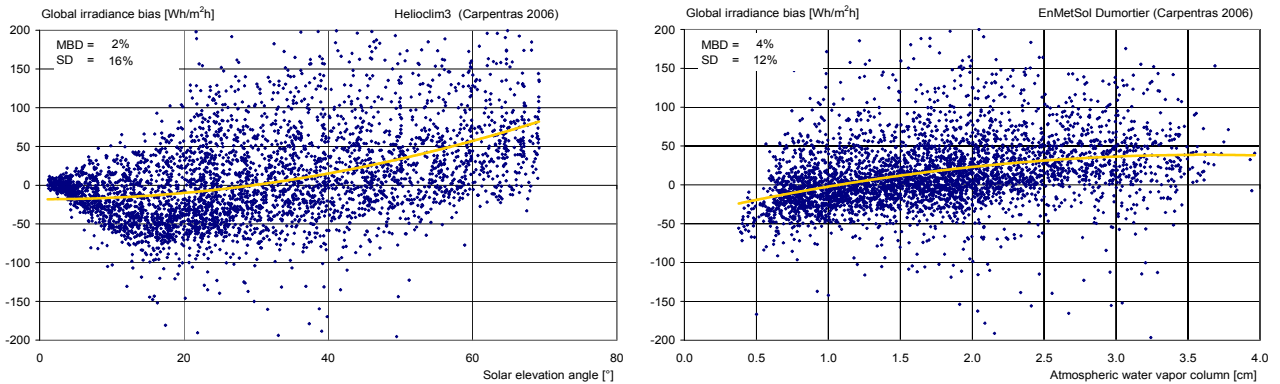


Figure 18 Global irradiance mean bias difference against the solar elevation angle (left) and the atmospheric water vapor content for two products and the site of Carpentras.

index is plotted against the solar elevation for all the products and the site of Carpentras on Figure 17. On these graphs, the clear sky conditions are represented by the upper boundary; it is interesting to point out that even if there is a great gap between the measurements and the modelled values for Helioclim, the overall performance is of the same order of magnitude than for the other products. It can also be noted here that for half of the products, the highest and the lowest modelled values of K_t are never reached.

To better understand the bias, a dependence analysis is done with the solar elevation angle and the water vapor column. To illustrate the results, two examples are given on Figure 18 where the bias is represented against the considered parameter, and a best fit is traced to underline the tendency. If the main pattern of all the models is to underestimate the global irradiance for low water vapor column values and overestimate it for high w , the bias pattern is variable from one model to the other with the solar elevation angle.

The study was also done with the turbidity, but this parameter was not available except for the sites of Carpentras and Sede Boquer, and on a daily basis. As for the water vapor content, the general tendency is a positive slope on the bias with the daily aerosol optical depth. An illustration for EnMetSol is given on Figure 19.

The irradiance for clear sky conditions is directly derived from the clear sky model. For

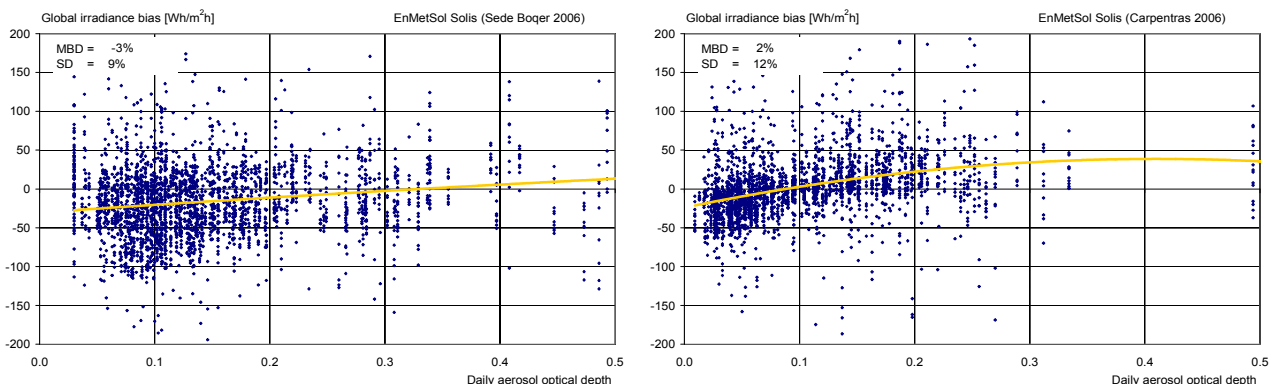


Figure 19 Global irradiance mean bias difference against the daily aerosol load of the atmosphere for the two sites of Sede Boquer and Carpentras.

			SolarGis		Heliosat 3v3		3Tier		EnMetSol (Solis)		EnMetSol (Dumortier)		IrSolAv	
sky type	G _h	nb	mbd	sd	mbd	sd	mbd	sd	mbd	sd	mbd	sd	mbd	sd
clear	498	35824	-9	43	-23	49	-18	57	-16	41	-16	43	-25	66
			-2%	9%	-5%	10%	-4%	11%	-3%	8%	-3%	9%	-7%	17%
intermediate	249	24096	12	67	22	75	12	80	20	60	19	61	19	95
			5%	27%	9%	30%	5%	32%	8%	24%	8%	25%	11%	53%
overcast	82	15917	18	49	39	65	42	62	25	48	24	48	36	79
			22%	60%	48%	80%	51%	75%	30%	58%	29%	59%	63%	138%

Table IV First order statistics in absolute and relative values for the global horizontal irradiance and for the three sky conditions. The absolute values are in [W/m²].

all sky condition, the clear sky model is combined with the cloud index. It is therefore interesting to differentiate the sky conditions following the rules defined in section 4. Table IV gives the overall results obtained for the three sky types. Without surprise, the clear sky conditions show the lowest standard deviation. All the algorithms have the same tendency to underestimate for clear conditions, and overestimate the global irradiance for intermediate and overcast conditions. Going more into details, the same tendency is also visible for all the sites. This is illustrated on Figure 20 for a cloudy (Lerwick) and a sunny (Carpentras) site. All the Figures and the complete Tables are given in the Annex.

The second order statistic given by the Kolmogorov-Smirnov index is a combination of

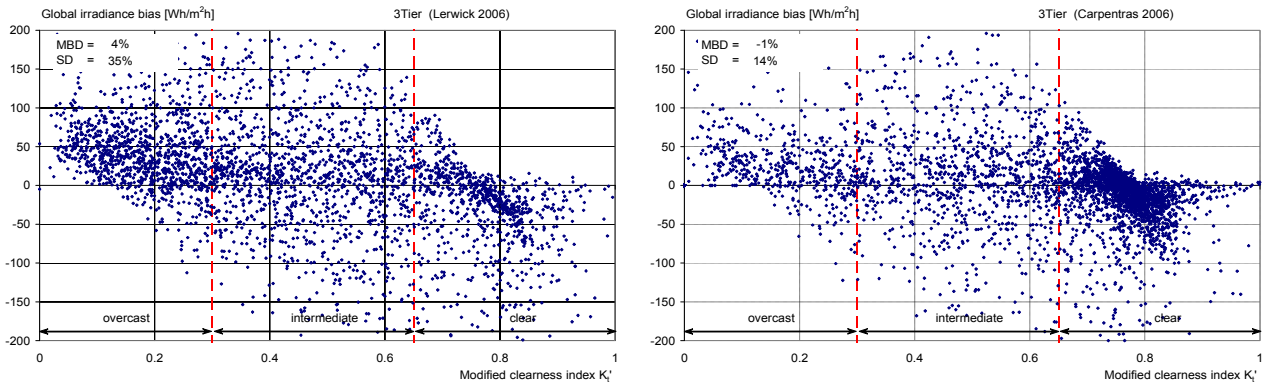


Figure 20 Global irradiance mean bias difference against the modified clearness index for the two sites of Lerwick and Carpentras.

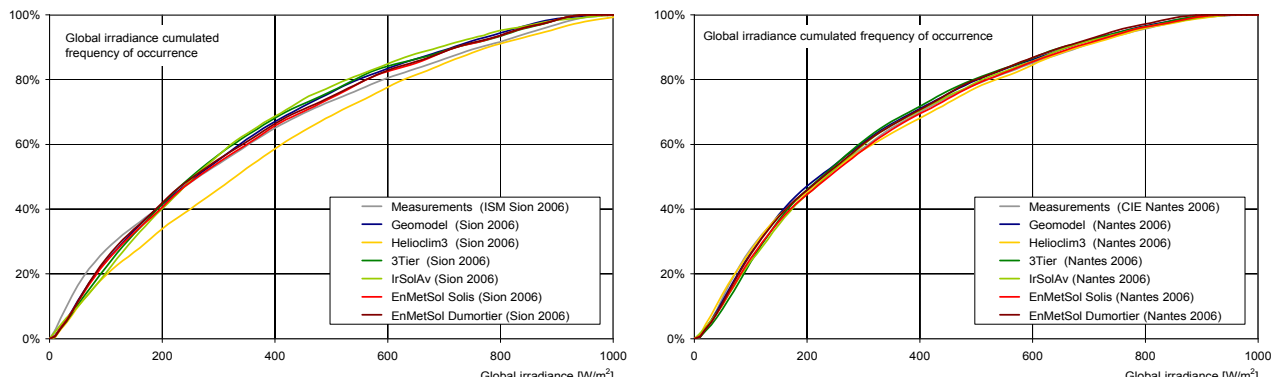


Figure 21 Clearness index cumulated frequency of occurrence for two sites with comparable standard deviation: Sion and Nantes.

the bias, the standard deviation (dispersion) and the cumulated frequency of occurrence. It is more sensitive and highlights smaller deviations than the first order indicators. This can be seen for example for the sites of Sion or Sede Boquer, where the standard deviation is similar to the other sites, but the clearness index frequency of occurrence shows discrepancies with the corresponding measurements. The cumulated frequency of occurrence for Sion and Nantes are given on Figure 21. The deviation from the measurements in Sion is visible for all the models at low and high irradiance levels; it can be due to snow in the Rhône Valley.

In conclusion, except for the four high altitude sites (potentially with snow), the average bias is around 1% ($4 \text{ [W/m}^2]$), positive for all the models. The best product derives the global irradiance with a standard deviation of 16% ($55 \text{ [W/m}^2]$).

Some models never reach the measured highest and lowest clearness index. The majority of the products show a bias dependance with the solar elevation angle, the water vapor column and when available, with the aerosol optical depth. In term of sky type, the general pattern is to underestimate the global irradiance for clear conditions, and to overestimate it for all the other conditions. Not all models take into account the snow, but even when included in the algorithm, the global irradiance for the concerned sites is not satisfactory.

8. Beam irradiance results

The same methodology is used for the validation of the beam irradiance component, except that the slots with no direct irradiance are excluded from the validation in order to avoid a bias in the overall statistic and a peak at zero irradiance in the frequency of occurrence.

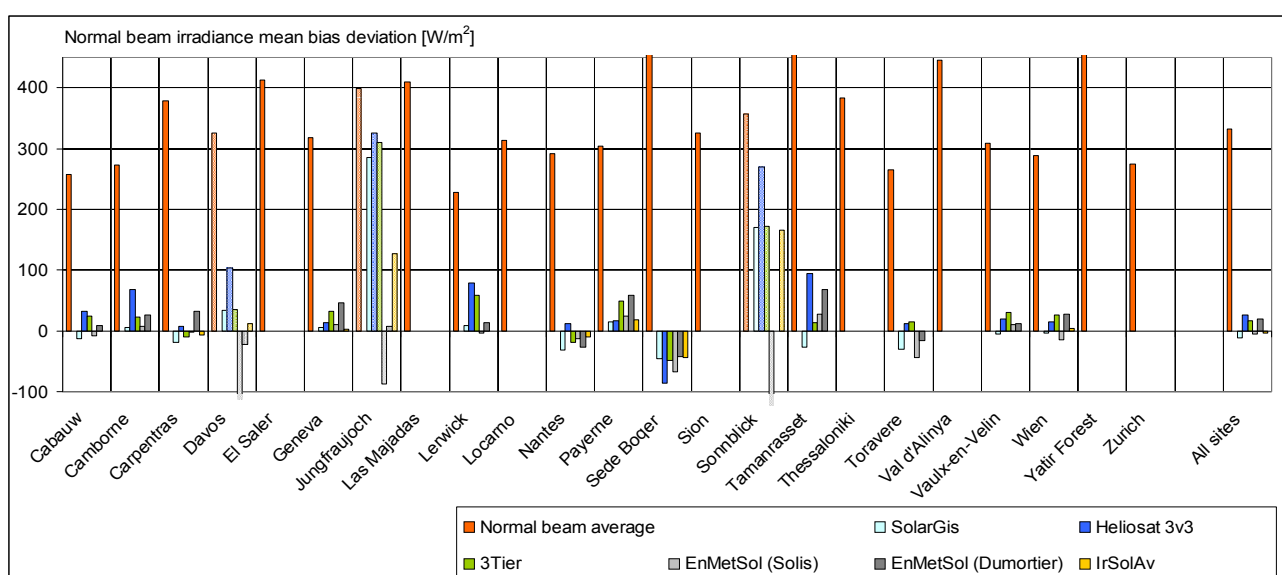


Figure 22 Average beam irradiance and absolute mean bias difference

	B_h [W/m ²]	nb	R ²	SolarGIS			R ²	Heliosat 3v3			R ²	3Tier			R ²	EmMetSol (Solis)			R ²	EmMetSol (Dumortier)			R ²	IrSolIAV			sd	KSI
				mbd	sd	KSI		mbd	sd	KSI		mbd	sd	KSI		mbd	sd	KSI		mbd	sd	KSI		mbd	sd	KSI		
Cabauw	220	4095	0.939	-13	93	28	0.877	32	130	28	0.868	24	136	14	0.931	-8	100	47	0.933	10	97	39						
Camborne	231	3471	0.942	6	96	28	0.885	68	134	26	0.896	22	129	20	0.937	7	101	46	0.940	27	98	31						
Carpentras	448	3993	0.936	-19	118	45	0.856	8	172	37	0.905	-9	141	30	0.924	-3	129	39	0.923	32	128	20	0.729	-6	237	28		
Davos	314	4200	0.864	34	187	94	0.748	104	247	108	0.707	35	271	113	0.735	-115	257	276	0.767	-23	244	190	0.663	12	291	153		
El Saler	307	3622	0.918	5	125	41	0.887	13	145	39	0.869	32	161	42	0.933	10	113	35	0.937	46	112	14	0.853	3	165	34		
Geneva	185	3311	0.541	285	360	158	0.327	326	373	216	0.461	310	381	174	0.319	-88	350	578	0.333	7	365	485	0.399	127	365	365		
Jungfraujoch																												
Las Majadas																												
Lerwick																												
Locarno																												
Nantes																												
Paveme																												
Sede Boquer																												
Sion																												
Sonnblick																												
Tamansasset																												
Thessaloniki																												
Toravere																												
Val d'Alinya																												
Vaulx-en-Velin																												
Wien																												
Yair Forest																												
Zurich																												
All sites	326	45590	n/a	-11	115	n/a	n/a	25	163	n/a	n/a	17	160	n/a	n/a	-5	128	n/a	n/a	19	125	n/a	n/a	-3	176	n/a		

Table V First and second order statistics in absolute values for the normal beam irradiance. The sites in grey are not taken into account in the overall statistics.

	B_h [W/m ²]	nb	R ²	SolarGIS			R ²	Heliosat 3v3			R ²	3Tier			R ²	EmMetSol (Solis)			R ²	EmMetSol (Dumortier)			R ²	IrSolIAV			sd	KSI
				mbd	sd%	KSI		mbd%	sd%	KSI		mbd	sd%	KSI		mbd%	sd%	KSI		mbd	sd%	KSI		mbd	sd%	KSI		
Cabauw	220	4095	0.939	-6	42	28	0.877	15	59	28	0.868	11	62	14	0.931	-4	45	47	0.933	4	44	39						
Camborne	231	3471	0.942	3	42	28	0.885	29	58	26	0.896	10	56	20	0.937	3	44	46	0.940	12	42	31						
Carpentras	448	3993	-4	26	45	28	0.856	2	38	37	0.905	-2	32	30	0.924	-1	29	39	0.923	7	29	20	0.729	-1	53	28		
Davos	314	4200	0.864	11	60	94	0.748	33	79	108	0.707	11	86	113	0.735	-36	82	276	0.757	-7	78	190	0.663	4	92	153		
El Saler	307	3622	0.918	2	41	41	0.887	4	47	39	0.869	10	52	42	0.933	3	37	35	0.937	15	36	14	0.853	1	54	34		
Geneva	185	3311	0.541	154	194	158	0.327	176	201	216	0.461	167	206	174	0.319	-48	189	578	0.333	4	197	485	0.399	69	197	365		
Jungfraujoch																												
Las Majadas																												
Lerwick																												
Locarno																												
Nantes																												
Paveme																												
Sede Boquer																												
Sion																												
Sonnblick																												
Tamansasset																												
Thessaloniki																												
Toravere																												
Val d'Alinya																												
Vaulx-en-Velin																												
Wien																												
Yair Forest																												
Zurich																												
All sites	326	45590	n/a	-4	35	n/a	n/a	8	50	n/a	n/a	5	49	n/a	n/a	-1	39	n/a	6	38	n/a	n/a	-1	54	n/a			

- 19 -

	B_h [W/m ²]	nb	R ²	SolarGIS			R ²	Heliosat 3v3			R ²	3Tier			R ²	EmMetSol (Solis)			R ²	EmMetSol (Dumortier)			R ²	IrSolIAV			sd	KSI
				mbd	sd%	KSI		mbd%	sd%	KSI		mbd	sd%	KSI		mbd%	sd%	KSI		mbd	sd%	KSI		mbd	sd%	KSI		
Cabauw	220	4095	0.939	-6	42	28	0.877	15	59	28	0.868</																	

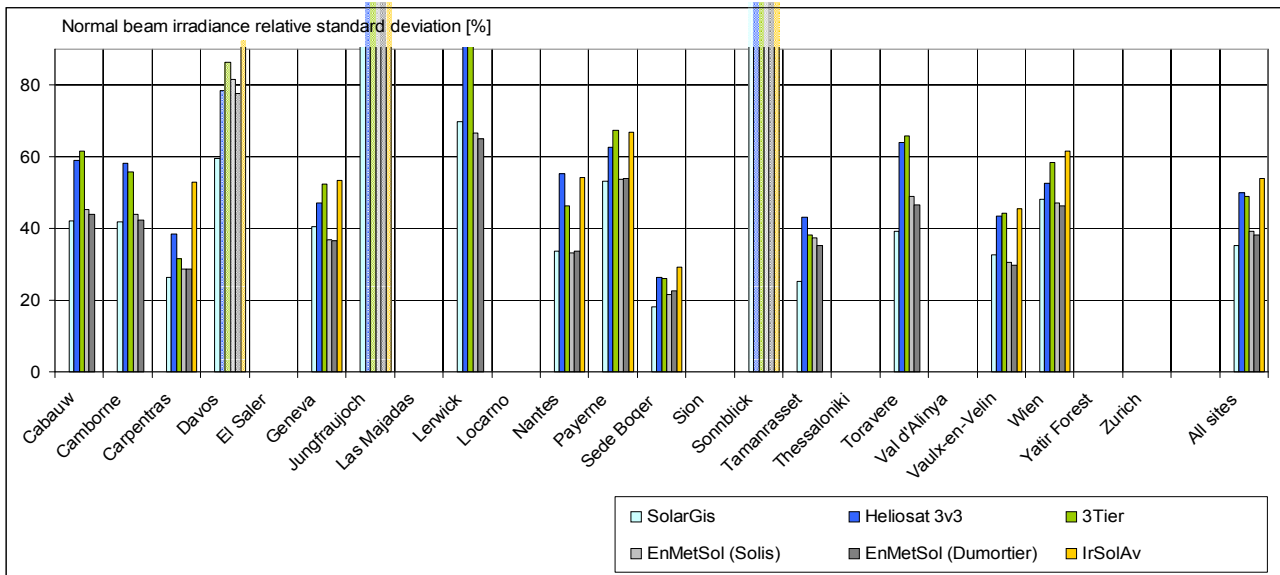


Figure 23 Relative standard deviation for the global irradiance.

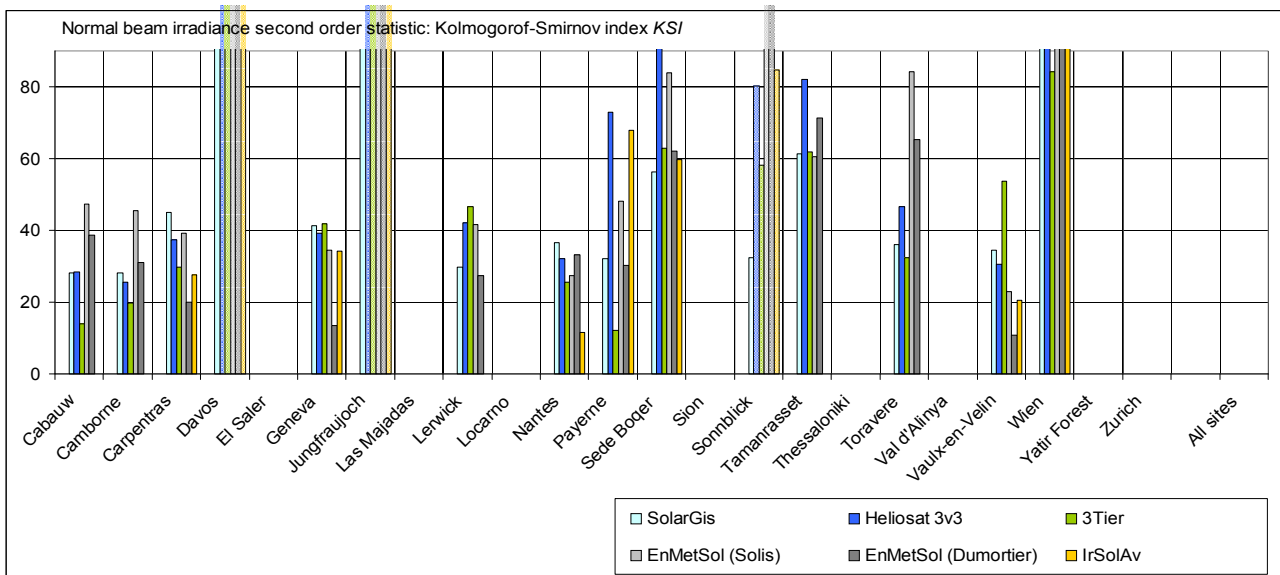


Figure 24 Second order statistics *KSI* for the global irradiance

The first and second statistics are given on Table V and VI, and on Figures 22 to 24. It can be seen on Figure 22 that the absolute bias for the beam component is variable from one site to the other, and depends on the product: for example, it is positive in Payerne (15-60 W/m²) and highly negative in Sede Boquer (-70 to -110 W/m²). For Tamanrasset, it varies from -27 [W/m²] (Geomodel) to +68 [W/m²] (EnMetSol) and +94 [W/m²] (Heliosat), and for Lerwick, from -4 to +78 [W/m²].

The standard deviation varies from 20% to 100%; it is highly variable in absolute and relative values. The site of Sede Boquer show the best values, but as it is a standard deviation, it doesn't take into account the its high mean bias. These deviation are illustrated on Figure 25, where on the left graph, the beam clearness index K_b is represented versus the solar elevation angle. It can be seen that the modelled clear sky upper limit never reaches the corresponding measurements. On the right graph, the

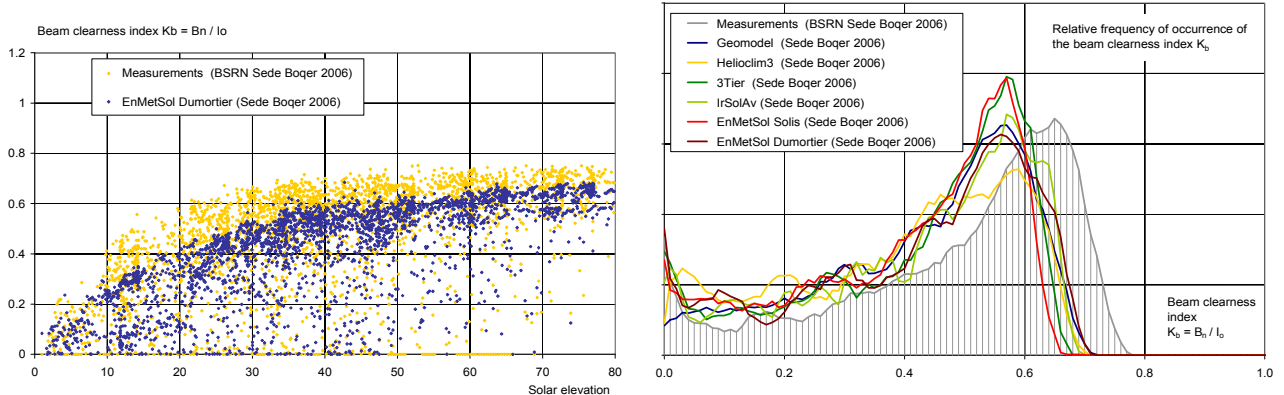


Figure 25 Beam clearness index versus the solar elevation angle, and the corresponding relative frequency of occurrence for the site of Sede Boquer.

frequency of occurrence is represented: the clear sky peak is too low for all the products. Part of the discrepancy can be an calibration issue. In fact, when comparing the BSRN beam ground measurements with the clear sky irradiance evaluated with solis from aeronet *aod* measurements, a 4% difference is visible as illustrated on Figure 26 (left: uncorrected, right: corrected by 4%). Also, inspecting BSRN data from Sede Boquer, a common 41 days sequence was found in data from 2005 and 2006. Comparison with satellite evaluated data conducted to eliminate this sequence from the present validation as it was much better reproduced with 2005 data. The 4% correction is already included in the above results.

The relative standard deviation is comparable for all the sites, except for Lerwick, the

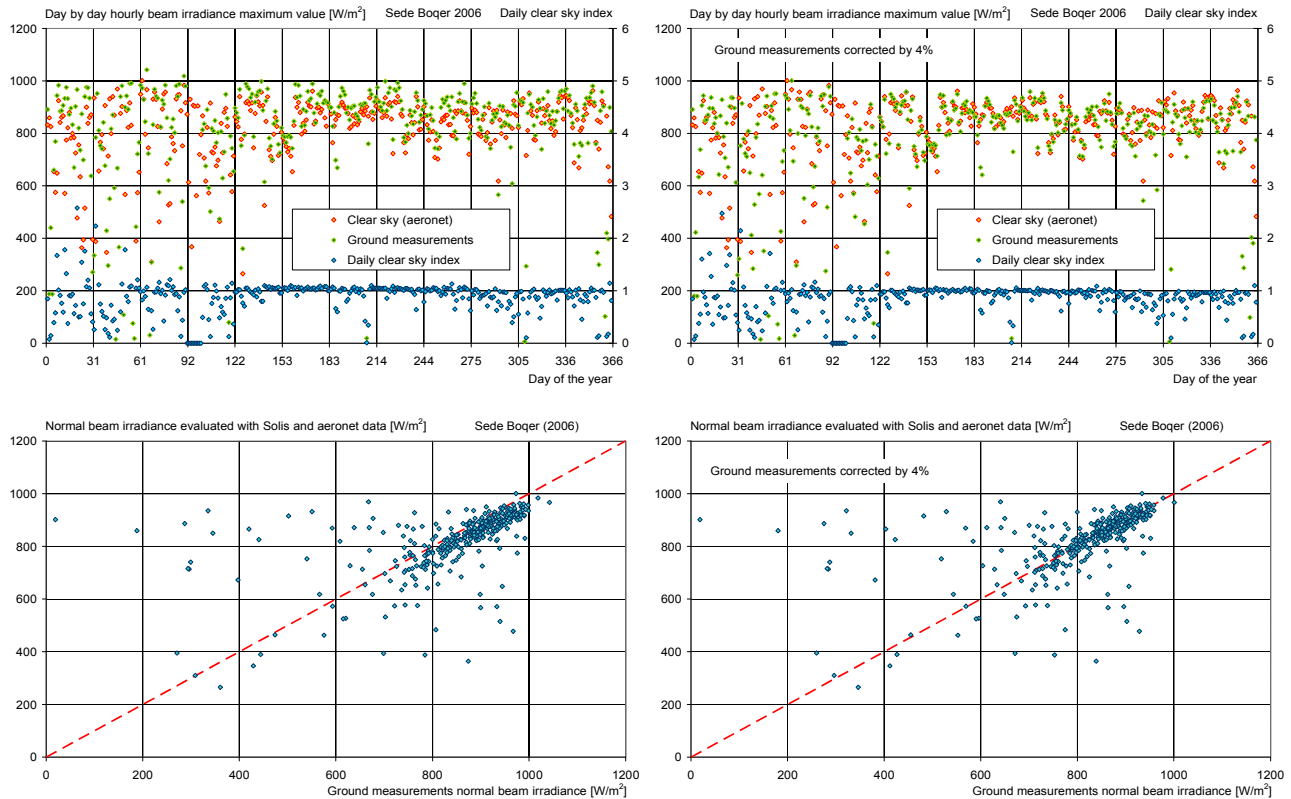


Figure 26 Sede Boquer beam irradiance before and after correction. On top, beam irradiance and clear sky index; bottom, daily measurements and evaluated data.

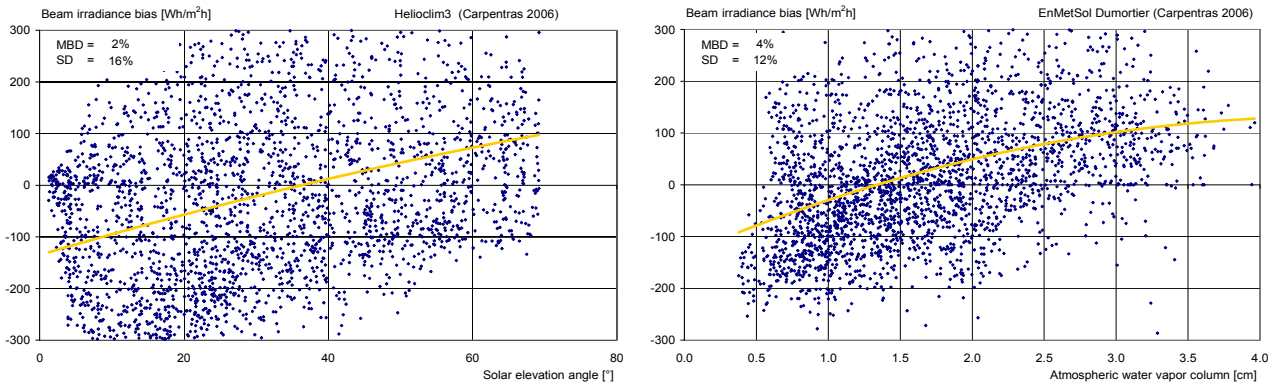


Figure 27 Normal beam irradiance mean bias difference against the solar elevation angle (left) and the atmospheric water vapor content (right) for the site of Carpentras.

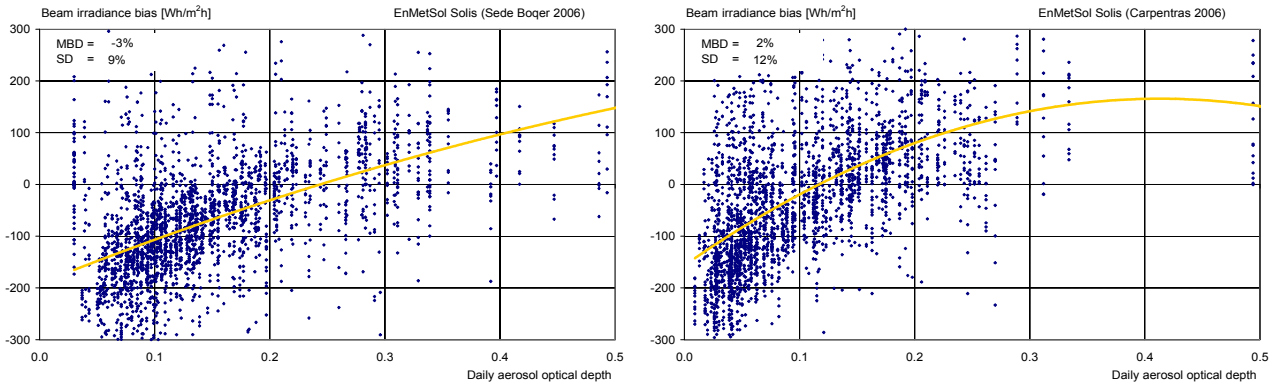


Figure 28 Normal beam irradiance mean bias difference against the daily aerosol load of the atmosphere for the two sites of Sede Boquer and Carpentras.

highest site in term of latitude, and where the average beam irradiance is very low. As for the global component, the results are good for the high latitude sites, and, due to the snow, not significative for the high altitude sites.

The same parameter dependance than for the global irradiance is conducted on the beam component. The results are given on Figures 27 and 28, where the same sites and models as for the global component are represented; they show very similar pattern (see Figures 18 and 19). This is a consequence of the method used to derive the beam irradiance: all the algorithm derive in a first step the global component, and split it into beam and diffuse with the help of a diffuse fraction model (Dirindex (Perez 1992) for SolarGis, Liu and Jordan (Liu 1960) for Helioclim, and in-house models for the other products). This means that the conclusion drawn for the global are also valid for the

			SolarGis		Heliosat 3v3		3Tier		EnMetSol (Solis)		EnMetSol (Dumortier)		IrSolAv	
sky type	B _n	nb	mbd	sd	mbd	sd	mbd	sd	mbd	sd	mbd	sd	mbd	sd
clear	627	20352	-66 -10%	121 19%	-61 -10%	163 26%	-45 -7%	161 26%	-66 -10%	138 22%	-24 -4%	137 22%	-83 -13%	179 29%
intermediate	142	15173	40 28%	110 78%	119 84%	146 103%	81 57%	163 115%	58 41%	108 76%	72 51%	114 81%	73 52%	171 120%
overcast	5	10065	14 302%	45 983%	51 1117%	70 1522%	38 831%	93 2022%	18 394%	50 1084%	18 393%	52 1129%	39 845%	89 1927%

Table VII First order statistics in absolute and relative values for the normal beam irradiance and for the three sky conditions. The absolute values are in [W/m²].

beam irradiance, even if the effects are more important due to the chained models.

The validation results for the three categories of the sky type are given on Table VII where the results for overcast conditions are included, even if they are not significative. Here again, comparable conclusions can be drawn, the bias is negative for clear conditions and positive for intermediate skies.

The above results are also visible on the second order statistic *KSI*, as illustrated on Figure 24 and 29, and given in Table V and VI. The fact that the beam is measured or retrieved from the global and the diffuse is not the main issue on the difference in the cumulated frequency of occurrence curves, it is more a site effect.

In conclusion, the beam irradiance is retrieved from the satellite images with an average standard deviation of 35% to 54% depending on the model. In term of irradiance value, it ranges from 90 to 200 [W/m²] according to the model and the site. The mean bias difference is slightly higher than for the global component, negative for clear conditions and positive for intermediate skies.

As the beam component is derived from the global, the dependances with the different parameters are similar but sharper than for the global irradiance.

9. Conclusions

The first conclusion is that the quality control is a key point in any model validation. Even if the data are highly qualified by the organisation in charge of the acquisition, uncertainties can remain in the data and influence the validation. The best case is when independent data such as aerosol optical depth are available.

The main conclusions of the present study are represented by the first order statistics:

- for latitude from 20° to 60°, altitude from sea level to 1800 m and various climate, the global irradiance is retrieved with a negligible bias and an average standard

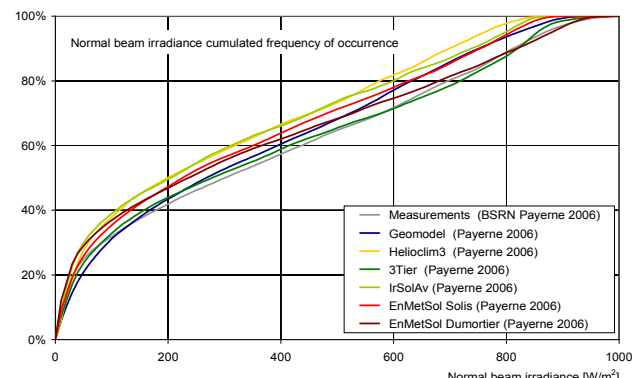
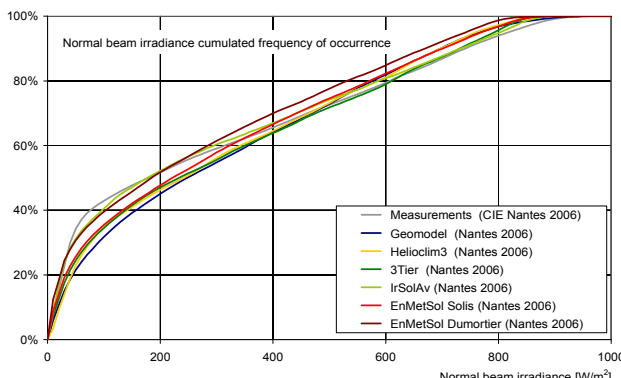


Figure 29 Beam clearness index cumulated frequency of occurrence for Nantes where the beam is retrieved from the diffuse, and Payerne where the beam component is acquired.

deviation around 16% for the best algorithm. For the beam irradiance, the bias is around several percents, and the standard deviation around 35%,

- as expected, the main dependance comes from the knowledge of the aerosol optical depth. A lower dependance with the atmospheric water vapor column and the solar elevation angle is pointed out,
- even if the snow cover is taken into account in the algorithm, the sites situated in high altitude such as Junfraujoch and Sonnblick give bad results and are not take into account in the overall statistic.
- the high latitude sites such as Cabauw, Camborne or Toravere give not poorer results than the other sites, only Lerwick, the highest site in latitude (60°N) presents more difficulties. It has also very low levels of irradiance,
- for the majority of the sites, SolarGis and EnMetSol give the best statistics for both of the components.

Nevertheless, the interannual variability of the irradiance conditions (it has been shown in a previous study that even for the same site and algorithm, the results can vary from one year to the other, Ineichen 2010a), the lack of independent ground measurements such as aerosol data, the difficulty to assess the exact calibration of the ground data, and the choice of a specific year to carry out the validation, conduct to results that give good indications, but from which it is difficult to draw general conclusions.

10. Acknowledgements

This comparative study could be performed thanks to the data provided by the FluxNet community (<http://www.fluxdata.org>), the Baseline Surface Radiation Network, the Aeronet network, the CSTB of Nantes and ENTPE in Vaulx-en-Velin, the World Radiation Data Center, and the Swiss Institute of Meteorology.

The derived products were kindly provided by Geomodel in Slovakia, 3Tier in Seattle, the Helioclim data bank in France, University of Oldenburg in Germany, and IrSolAv company in Spain.

11. Nomenclature and abbreviations

I_o	solar constant in W/m ²
B_n	direct normal incidence irradiance in W/m ²
G_h	surface solar global irradiance on a horizontal plane in W/m ²
G_{hc}	clear sky surface solar irradiance in W/m ²
D_h	surface solar diffuse irradiance on a horizontal plane in W/m ²
K_t	global or surface solar irradiance clearness index
K_b	beam clearness index
K_c	clear sky index
K_h	daily global clear sky index
K_{hb}	daily beam clear sky index
n	cloud index
$F_c(G_h)$	cumulated frequency of occurrence of the global irradiance
h	solar elevation or altitude angle in degrees (°)
AM	optical air mass
RTM	radiative transfer model
T_L	Linke turbidity
aod	aerosol optical depth, or atmospheric aerosol load
T_a	surface (ambient) temperature
HR	relative humidity
w	atmospheric total water vapour column
mbd	mean bias difference
$rmsd$	root mean square difference
sd	standard deviation
KSI	Kolmogorov-Smirnov index, second order statistic

12. References

Aeronet (AErosol RObotic NETwork) program, <http://aeronet.gsfc.nasa.gov/>

Atwater M.A., Ball J.T. (1976) Comparison of radiation computations using observed and estimated precipitable water. *Appl. Meteorol.* 15, 1319-1320

Beyer HG, Costanzo C, Heinemann D (1996): Modifications of the Heliosat procedure for irradiance estimates from satellite data. *Solar Energy* 56, 207-212.

Black J.N., Bonython C.W., Prescott J.A. (1954) *Solar radiation and the duration of sunshine*. Quart. J. Roy. Met. Soc. 80, pp231-235

Dagestad, K. F. and Olseth, J. A., (2007). A modified algorithm for calculating the cloud index. *Solar Energy*. 81, 280-289.

Derrien M., H. Gleau (2005) MSG/SEVIRI cloud mask and type from SAFNWC, *International Journal of Remote Sensing*, 26, 4707-4732.

DUMORTIER D (1998): The Satellite model of turbidity variations in Europe. Technical Report

Dürr B., Philipona R, (2004) *Automatic cloud amount detection by surface longwave downward radiation measurements*. J. Geoph. Res., Vol 109

Dürr B. (2006) , personal communication

Espinar B, Ramirez L, Drews D, Beyer H.G, Zarzalejo L.F, Polo J, Martin L. (2009) Analysis of different comparison parameters applied to solar radiation data from satellite and German radiometric stations, *Solar Energy* 83 (2009) 118-125

ESRA (2000) The european solar radiation atlas. Coordinators : K. SCHARMER, J. GREIF, ISBN : 2-911762-21-5

Fontoynont M, Dumortier D et al. (1998) Satellight: A WWW server which provides high quality daylight and solar radiation data for Western and Central Europe. 9th Conference on Satellite Meteorology and Oceanography, 434-437. Frouin R. A., Chertock B., (1992). A technique for global monitoring of net solar irradiance at the ocean surface. Part 1 : Model, *Journal of Applied meteorology*, 31,pp. 1056-1066.

Hammer A, Heinemann D, Hoyer C, Kuhleman R, Lorenz E, Müller R, Beyer HG (2003): Solar energy assessment using remote sensing technologies. *Remote Sensing of Environment*, 86, 423-432.

Hammer A, Lorenz E, Kemper A, Heinemann D, Beyer HG, Schumann K, Schwandt M (2009): 'Direct normal irradiance for CSP based on satellite images of Meteosat Second Generation', SolarPACES 2009, Berlin

Helioclim (2009) Sun radiation atlas based on processing of Meteosat data.
<<http://www.helioclim.net/>>

Ineichen P, Perez R. (2002) A new airmass independent formulation for the Linke turbidity coefficient. *Solar Energy* **73**, No. 3, 151–157

Ineichen P. (2008c). Comparison and validation of three global-to-beam irradiance models against ground measurements. *Sol. Energy* , doi:10.1016/j.solener.2007.12.006

Ineichen P. (2008a) A broadband simplified version of the Solis clear sky model, *Solar Energy* 82, pp 758–762

Ineichen P. (2008b) Conversion function between the Linke turbidity and the atmospheric water vapor and aerosol content, *Solar Energy* 82, pp. 1095–1097

Ineichen P. (2008c). Comparison and validation of three global-to-beam irradiance models against ground measurements. *Sol. Energy* , doi:10.1016/j.solener.2007.12.006

Ineichen P., Barroso C., Geiger B., Hollmann R., Marsouin A., Mueller R. (2009) Satellite Application Facilities irradiance products: hourly time step comparison and validation over Europe. *International Journal of Remote Sensing*, Vol. 30, No. 21, pp. 5549–5571

Ineichen P., Perez R. (2010). Aerosol quantification based on global irradiance. *Solar paces proceedings*, 21-24 sept. Perpignan, France. Available from:
[http://www.cuepe.ch/html/biblio/pdf/ineichen_2010_aerosol_quantification\(SP\).pdf](http://www.cuepe.ch/html/biblio/pdf/ineichen_2010_aerosol_quantification(SP).pdf)

Ineichen P. (2010). Interannual variability and global irradiance evaluation. IEA Task XXXVI report. Available from:

http://www.cuepe.ch/html/biblio/pdf/ineichen_2010_05_interannual_variability.pdf

Kalnay E et al. (1996): The NMC/NCAR 40-year reanalysis project. *Bull. Am. Meteorol. Soc.* 77 (3), 437–472.

Kasten F. (1980) A simple parameterization of two pyrheliometric formulae for determining the Linke turbidity factor. *Meteor. Rdsch.* **33**, 124–127.

Kinne, S. et al (2005) An AeroCom initial assessment optical properties in aerosol component modules of global models *Atmos. Chem. Phys. Discuss.*, **5**, 1-46.

Linke F. (1922) Transmissions-koeffizient und Trübungsfaktor. Beitr. Phys. Fr. Atmos. 10, pp 91-103.

Liu B.Y.H, Jordan R.C (1960) The interrelationship and characteristic distribution of direct, diffuse and total solar radiation. Volume 4, Issue 3, Pages 1-19

Lorenz E. (2007): Improved diffuse radiation model, MSG. Report for the EC-project PVSAT-2: Intelligent Performance Check of PV System Operation

Louche, A., Notton, G., Poggi, P. and Simonnot, G., (1991). Correlations for direct normal and global horizontal irradiation on a French Mediterranean site. Solar Energy. 46, 261-266.

Mueller R.W. et al, (2004) Rethinking satellite based solar irradiance modelling – The SOLIS clear sky module. Remote Sensing of Environment, **91**, 160-174.

Perez R., R. Seals, P. Ineichen, R. Stewart, D. Menicucci (1987) A New Simplified Version of the Perez Diffuse Irradiance Model for Tilted Surfaces. Description Performance Validation. Solar Energy, 39, 221-232.

Perez R., Ineichen P., Seals R., Zelenka A. (1990) *Making full use of the clearness index for parametrizing hourly insolation conditions*. Solar Energy, Vol. 45, N° 2, pp. 111-114.

Perez R., P. Ineichen, E. Maxwell, R. Seals, A. Zelenka (1992) Dynamic global to direct irradiance conversion models. ASHARE Trans. Res. Series, 1992, 354-369

Perez R., P. Ineichen, K. Moore, M. Kmiecik, C. Chain, R. George, F. Vignola (2002) A New Operational Satellite-to-Irradiance Model, Solar Energy, 73, 2002, 307-317.

Polo, J., Zarzalejo, L. F., Martin, L., Navarro, A. A. and Marchante, R., (2009a) Estimation of daily Linke turbidity factor by using global irradiance measurements at solar noon. Solar Energy. 83, 1177-1185.

Polo, J., Zarzalejo, L. F., Salvador, P. and Ramírez, L. (2009b) Angstrom turbidity and ozone column estimations from spectral solar irradiance in a semi-desertic environment in Spain. Solar Energy. 83, 257-263.

Randel D., T. H Vonder Haar, M.A. Ringerrud, G. L. Stephens, T.J. Greenwald C.L. Combs (1996) A New Global Water Vapour Dataset. Bulletin of the American Meteorological Society, 77, 1233-1246.

Remund J. (2008), Updated Linke Turbidity and aerosol optical depth climatologies, IEA SHC Task 36 expert meeting, June 2008, Wels, Austria.

Remund J. (2009): Aerosol optical depth and Linke turbidity climatology, Description for final report of IEA SHC Task 36, Meteotest Bern

Rigollier C., Bauer O., Wald L. (2000) On the Clear Sky Model of the ESRA - european Solar Radiation Atlas - with Respect to the Heliosat Method. *Solar Energy* **68** (1), 33-48.

Rigollier C., Lefèvre M, Wald L. (2004) The method heliosat-2 for deriving shortwave solar irradiance radiation from satellite images *Solar Energy*, 77(2), 159-169

Ruiz-Arias J.A., T. Cebecauer, J. Tovar-Pescador, M. Šúri, (2010). Spatial disaggregation of satellite-derived irradiance using a high resolution digital elevation model, accepted to *Solar Energy*.

Ruyter de Wildt M., G. Seiz, A. Gruen (2007) Operational snow mapping using multitemporal Meteosat SEVIRI imagery, *Remote Sensing of Environment*, 109, 29-41.

WMO Publication N° 8 (2008) Guide to Meteorological Instruments and Methods of Observation, ISBN 978-92-63-100085

Zarzalejo, L. F., Polo, J., Martín, L., Ramírez, L. and Espinar, B. (2009). A new statistical approach for deriving global solar radiation from satellite images. *Solar Energy*. 83, 480-484.

Zelenka A, Perez R, Seals R, Renne D (1999) Effective Accuracy of Satellite-Derived Hourly irradiance. *Theor. Appl. Climatol.* 62, 199-207

Annexe: figures in the following pages:

For the clear, intermediate and overcast sky conditions:

- First and second order statistics in absolute values for the global horizontal irradiance. The sites in grey are not taken into account in the overall statistics.
- First and second order statistics in relative values for the global horizontal irradiance. The sites in grey are not taken into account in the overall statistics.
- First and second order statistics in absolute values for the normal beam irradiance. The sites in grey are not taken into account in the overall statistics.
- First and second order statistics in relative values for the normal beam irradiance. The sites in grey are not taken into account in the overall statistics.

Global irradiance

Clear sky conditions:

$$0.65 < K'_t \leq 1.00$$

	G ₁ [W/m ²]	nb	R ²	mbd	sd	R ²	mbd	sd	R ²	mbd	sd	R ²	mbd	sd	R ²	mbd	sd	R ²	mbd	sd
Cabauw	420	1374	0.980	-17	50	0.983	-33	50	0.976	-24	55	0.986	-23	42	0.985	-25	44	0.985	-25	44
Camborne	459	1362	0.985	-25	46	0.986	-34	47	0.976	-36	57	0.990	-27	36	0.990	-28	36	0.990	-28	36
Centrastras	481	2522	0.993	-5	32	0.981	-15	44	0.988	-16	42	0.994	-8	31	0.993	0	34	0.921	-34	107
Davos	517	1775	0.954	-39	76	0.970	-47	64	0.975	-53	109	0.948	-101	81	0.935	-70	92	0.832	-82	148
El Saler	549	2027	0.980	-11	52	0.987	-24	48	0.972	-25	60	0.985	-7	44	0.985	-14	44	0.978	-40	52
Geneva	508	1464	0.983	0	46	0.983	-24	51	0.966	-8	67	0.987	2	40	0.986	12	45	0.957	-25	74
Jungfraujoch	600	1558	0.930	-39	105	0.982	-100	98	0.983	-100	168	0.685	-301	199	0.675	-262	206	0.768	-186	179
Las Majadas	539	2022	0.988	13	42	0.980	-1	43	0.983	12	52	0.991	18	37	0.982	6	35	0.982	-3	51
Lerwick	402	874	0.970	-40	58	0.972	-45	60	0.950	-43	75	0.977	-39	51	0.976	-44	52	0.972	-39	55
Locarno	512	1813	0.982	-3	44	0.985	-23	52	0.968	-9	63	0.984	-5	42	0.980	-12	47	0.972	-39	68
Nantes	456	1542	0.982	-20	48	0.978	-38	56	0.972	-31	59	0.988	-17	40	0.987	-33	42	0.964	-28	68
Payerne	504	1539	0.977	-13	55	0.972	-46	64	0.964	-22	70	0.980	-14	52	0.978	-4	56	0.958	-36	73
Sede Boquer	662	2285	0.989	-6	38	0.988	-46	41	0.975	-34	59	0.989	-27	41	0.988	-35	43	0.979	-43	55
Sion	535	1851	0.957	-35	71	0.977	-9	58	0.941	-46	83	0.979	-31	50	0.972	-38	57	0.846	-60	133
Sombrück	481	1837	0.921	-35	99	0.946	-38	83	0.870	-53	134	0.790	-185	150	0.774	-139	162	0.847	-49	140
Tamanassett	621	3154	0.994	-11	34	0.980	4	51	0.985	-2	55	0.992	-14	39	0.992	-15	37	0.973	-29	60
Thessaloniki	536	2025	0.989	-7	38	0.988	-34	43	0.977	-30	63	0.978	-28	55	0.973	-30	55	0.973	-29	60
Toravere	400	1545	0.985	-16	41	0.988	-33	68	0.968	-27	58	0.983	-25	43	0.978	-24	48	0.966	11	75
Val d'Alinya	578	1532	0.985	-15	48	0.985	-3	57	0.979	-11	60	0.986	-48	49	0.986	-26	47	0.966	11	75
Vaulx-en-Velin	514	1468	0.985	1	43	0.984	-20	47	0.973	-22	59	0.987	-3	40	0.987	-4	40	0.973	-16	57
Wien	460	1551	0.981	-12	48	0.983	-33	48	0.972	-22	59	0.986	-22	41	0.986	-12	42	0.956	-29	73
Yatir Forest	626	2523	0.993	-12	33	0.993	-31	40	0.987	-28	45	0.994	-34	29	0.994	-31	31	0.982	-28	51
Zurich	465	1351	0.975	-9	60	0.973	-32	68	0.963	-14	74	0.972	-19	62	0.971	-5	68	0.956	-26	76
All sites	498	35824	-9	43	-23	49	-18	57	-16	41	-16	41	-16	43	-16	43	-25	43	-25	66

Clear sky conditions: first and second order statistics in absolute values for the global horizontal irradiance. The sites in grey are not taken into account in the overall statistics.

	GHI [W/m ²]	nb	R ²	mbd	sd%	R ²	mbd%	sd%	R ²	mbd%	sd%	R ²	mbd%	sd%	R ²	mbd%	sd%	R ²	mbd%	sd%	
Cabauw	420	1374	0.980	-4	12	0.983	-8	12	0.976	-6	13	0.986	-5	10	0.985	-6	10	0.985	-6	10	
Camborne	459	1362	0.985	-5	10	0.986	-7	10	0.976	-8	13	0.990	-6	8	0.990	-6	8	0.990	-6	8	
Centrastras	481	2522	0.993	-1	7	0.991	-3	9	0.988	-3	9	0.994	-2	6	0.993	0	7	0.921	-7	22	
Davos	517	1775	0.954	-7	15	0.970	-9	12	0.915	-10	21	0.948	-20	16	0.935	-14	18	0.832	-16	29	
El Saler	549	2027	0.980	-2	9	0.987	-4	9	0.972	-5	11	0.985	-1	8	0.985	-3	8	0.978	-7	10	
Geneva	508	1464	0.983	0	9	0.983	-5	10	0.966	-2	13	0.987	0	8	0.986	2	9	0.957	-5	15	
Jungfraujoch	600	1558	0.930	-6	18	0.932	-17	16	0.831	-11	28	0.685	-50	33	0.675	-44	34	0.768	-31	30	
Las Majadas	539	2022	0.988	2	8	0.980	0	8	0.983	-2	10	0.991	3	7	0.992	1	7	0.982	-1	9	
Lerwick	402	874	0.970	-10	14	0.972	-11	15	0.950	-11	19	0.977	-10	13	0.976	-11	13	0.972	-8	11	
Locarno	512	1813	0.982	-1	9	0.985	-5	10	0.968	-2	12	0.984	-1	8	0.980	-2	9	0.964	-6	11	
Nantes	456	1542	0.982	-4	11	0.978	-8	12	0.972	-7	13	0.988	-4	9	0.987	-7	11	0.958	-7	15	
Payerne	504	1539	0.977	-2	11	0.972	-9	13	0.964	-4	14	0.980	-3	10	0.979	-1	11	0.979	-7	15	
Sede Boquer	662	2285	0.989	-1	6	0.988	-7	6	0.975	-5	9	0.989	-4	6	0.988	-5	6	0.979	-7	8	
Sion	535	1851	0.957	-7	13	0.977	-2	11	0.941	-9	16	0.979	-6	9	0.972	-7	7	0.846	-11	25	
Sombrück	481	1837	0.921	-21	946	-8	870	-11	78	0.790	-38	31	0.774	-29	34	0.847	-10	29	0.847	-10	29
Tamanassett	621	3154	0.994	-2	6	0.990	1	8	0.985	0	9	0.992	-2	6	0.992	-2	6	0.973	-5	11	
Thessaloniki	536	2025	0.989	-1	7	0.988	-6	8	0.971	-6	12	0.977	-6	10	0.979	-6	12	0.973	-5	11	
Toravere	400	1545	0.985	-4	10	0.988	-8	17	0.968	-7	14	0.983	-6	6	0.983	-6	6	0.979	-7	15	
Val d'Alinya	578	1468	0.985	-3	8	0.985	0	10	0.979	-2	10	0.985	-8	9	0.986	-5	8	0.966	2	13	
Wien	514	1551	0.981	-3	10	0.984	-4	9	0.973	0	11	0.987	1	8	0.987	-1	8	0.973	-3	11	
Yatir Forest	626	2523	0.993	-2	5	0.983	-5	6	0.987	-4	7	0.994	-6	5	0.984	-5	5	0.982	-4	8	
Zurich	465	1351	0.975	-2	13	0.973	-7	15	0.963	-3	16	0.972	-4	13	0.971	-1	15	0.956	-6	16	
All sites	498	35824	-2	9	-5	10	-4	11	-3	8	-3	8	-3	9	-3	9	-7	7	-7	17	

Clear sky conditions: first and second order statistics in relative values for the global horizontal irradiance. The sites in grey are not taken into account in the overall statistics.

Beam irradiance

Clear sky conditions

$$0.65 < K'_t \leq 1.00$$

	B_n [W/m ²]	nb	SolarGIS			Heliosat 3v3			3Tier			EnMetSol (Soilis)			EnMetSol (Dumontier)			IrSoIAv		
			R2	mbd	sd%	R2	mbd	sd%	R2	mbd	sd%	R2	mbd	sd%	R2	mbd	sd%	R2	mbd	sd%
Cabauw	530	1335	0.884	-64	112	0.829	-51	139	0.820	-35	141	0.867	-79	115	0.865	-33	118	0.888	-19	109
Camborne	556	1195	0.894	-49	109	0.828	-11	141	0.824	-36	144	0.881	-63	114	0.888	-11	116	0.684	-91	202
Carpentras	652	2522	0.901	-63	100	0.827	-70	141	0.870	-57	119	0.867	-52	115	0.868	-8	116	0.393	-125	348
Davos	676	1775	0.742	-49	202	0.525	-55	263	0.599	-63	328	0.423	-307	288	0.463	-149	306	0.393	-125	452
EI Saler	631	1464	0.805	-51	129	0.775	-83	139	0.750	-20	159	0.815	-43	123	0.834	21	122	0.724	-90	165
Geneva	381	1558	0.393	363	445	0.325	206	446	0.443	286	440	0.286	-254	444	0.294	-130	460	0.343	46	452
Jungfraujoch																				
Las Majadas																				
Lerwick	491	790	0.839	-68	138	0.783	-29	170	0.712	-31	190	0.849	-99	134	0.858	-49	130			
Locarno																				
Nantes	595	1542	0.875	-83	107	0.781	-92	147	0.794	-79	144	0.868	-68	108	0.861	-88	107	0.748	-85	168
Payerne	585	1539	0.709	-33	177	0.655	-72	193	0.648	5	210	0.662	-20	189	0.695	42	184	0.629	-60	206
Sede Boquer																				
Sion	757	2247	0.824	-97	101	0.666	-141	153	0.628	-105	148	0.722	-121	126	0.704	-92	134	0.540	-102	171
Sonneblick																				
Tamanrasset	518	1837	0.595	150	312	0.405	133	366	0.372	65	402	0.322	-318	364	0.299	-148	418	0.392	82	409
Thessaloniki	706	3154	0.904	-74	112	0.702	24	204	0.733	-41	186	0.756	-33	174	0.790	13	161			
Toraverne	582	1545	0.875	-84	119	0.740	-98	194	0.757	-78	167	0.815	-135	137	0.810	-83	145			
Val d'Alnya																				
Vaulx-en-Velin	643	1468	0.869	-57	99	0.801	-71	120	0.796	-9	134	0.846	-33	105	0.866	-28	101	0.781	-74	136
Wien	541	1551	0.760	-40	159	0.786	-56	151	0.721	-13	176	0.761	-75	154	0.768	6	155	0.707	-65	180
Yatir Forest																				
Zurich																				
All sites	627	20352	-66	121	-61	163	-45	161	-61	163	-45	161	-66	138	-24	137	-83	179		

Clear sky conditions: first and second order statistics in absolute values for the normal beam irradiance. The sites in grey are not taken into account in the overall statistics.

	B_n [W/m ²]	nb	SolarGIS			Heliosat 3v3			3Tier			EnMetSol (Soilis)			EnMetSol (Dumontier)			IrSoIAv		
			R2	mbd%	sd%	R2	mbd%	sd%	R2	mbd%	sd%	R2	mbd%	sd%	R2	mbd%	sd%	R2	mbd%	sd%
Cabauw	530	1335	0.884	-12	21	0.829	-10	26	0.820	-7	27	0.867	-15	22	0.865	-6	22			
Camborne	556	1195	0.894	-9	20	0.826	-2	25	0.824	-6	26	0.881	-11	21	0.888	-3	20			
Carpentras	652	2522	-10	15	0.827	-11	22	0.870	-9	18	0.867	-8	18	0.868	-1	18				
Davos	676	1775	-7	30	0.525	-8	39	0.399	-12	49	0.423	-45	43	0.463	-22	45				
EI Saler	631	1464	0.805	-8	20	0.775	-13	22	0.750	-3	25	0.815	-7	20	0.834	3	19	0.724	-14	26
Geneva	381	1558	0.393	95	117	0.325	54	117	0.443	70	116	0.286	-67	117	0.294	-34	121	0.343	12	119
Jungfraujoch																				
Las Majadas																				
Lerwick	491	790	0.839	-14	28	0.783	-6	35	0.712	-6	39	0.849	-20	27	0.858	-10	27			
Locarno																				
Nantes	595	1542	-14	18	0.781	-15	25	0.794	-13	24	0.868	-11	18	0.861	-15	18	0.748	-14	28	
Payerne	585	1539	-6	30	0.655	-12	33	0.648	1	36	0.662	-3	32	0.695	7	31	0.629	-10	35	
Sede Boquer																				
Sion																				
Sonneblick	518	1837	0.595	29	60	0.405	26	71	0.372	12	78	0.322	-61	70	0.299	-29	81	0.392	16	79
Tamanrasset	706	3154	-10	16	0.702	3	29	0.733	-6	26	0.756	-5	25	0.790	2	23				
Thessaloniki																				
Toraverne	582	1545	-14	21	0.740	-17	33	0.757	-13	29	0.815	-23	23	0.810	-14	25				
Val d'Alnya																				
Vaulx-en-Velin	643	1468	-9	15	0.801	-11	19	0.796	-1	21	0.846	-5	16	0.866	-4	16	0.781	-11	21	
Wien	541	1551	-7	29	0.786	-10	28	0.721	-2	32	0.761	-14	28	0.768	1	29	0.707	-12	33	
Yatir Forest																				
Zurich																				
All sites	627	20352	-10	19	-10	26	-7	26	-10	26	-7	26	-10	22	-4	22	-13	22	-13	29

Clear sky conditions: first and second order statistics in relative values for the normal beam irradiance. The sites in grey are not taken into account in the overall statistics.

Global irradiance

Intermediate sky conditions $0.30 < K'_{t} \leq 0.65$

	$G_h [\text{W/m}^2]$	nb	SolarGIS			Heliosat 3v3			3Tier			EnMetSol (Soilis)			EnMetSol (Dumontier)			IrSoIAV		
			R ²	mbd	sd%	R ²	mbd	sd%	R ²	mbd	sd%	R ²	mbd	sd%	R ²	mbd	sd%	R ²	mbd	sd%
Cabauw	252	1578	0.950	-9	54	0.951	-1	60	0.919	0	69	0.970	3	43	0.968	0	44			
Camborne	249	1546	0.941	1	60	0.963	16	58	0.913	2	72	0.962	12	50	0.963	10	49	0.779	27	137
Carpentras	267	986	0.937	21	71	0.966	41	68	0.929	12	71	0.964	35	56	0.965	39	59	0.693	-8	141
Davos	235	1571	-5	100	0.948	62	82	0.861	15	101	0.887	-26	81	0.887	-12	87				
El Saler	304	1083	0.919	22	82	0.953	37	77	0.908	10	84	0.942	34	70	0.943	29	69	0.898	14	87
Geneva	266	1208	0.935	20	67	0.952	15	67	0.898	10	83	0.958	27	55	0.958	30	58	0.868	19	95
Jungfraujoch	270	1220	0.763	4	146	0.917	123	118	0.773	72	148	0.739	-65	121	0.734	-38	130	0.564	11	189
Las Majadas	292	1036	0.925	34	81	0.957	57	75	0.900	28	90	0.947	56	74	0.949	47	71	0.893	38	93
Lerwick	234	1307	0.933	0	57	0.937	19	74	0.870	13	81	0.938	-7	54	0.938	-10	54			
Locarno	258	1199	0.944	24	64	0.958	50	80	0.928	32	77	0.963	37	56	0.962	33	57	0.901	23	84
Nantes	264	1595	0.958	-1	55	0.938	18	81	0.928	-1	72	0.973	14	46	0.973	4	45	0.896	12	91
Payerne	247	1398	0.942	12	62	0.933	-2	71	0.904	10	79	0.957	21	66	0.957	25	59	0.867	10	92
Sede Boquer	274	522	0.931	30	75	0.946	5	77	0.878	2	89	0.944	28	68	0.944	19	64	0.900	26	86
Sion	224	1437	0.907	-2	75	0.964	62	73	0.905	-1	76	0.953	12	56	0.950	8	58	0.771	3	116
Sonneblick	287	1570	0.765	9	156	0.901	106	125	0.777	54	158	0.767	-51	128	0.761	-15	141	0.661	29	183
Tamanrasset	313	915	0.954	41	80	0.962	95	108	0.921	56	113	0.956	78	98	0.957	76	95			
Thessaloniki	260	1036	0.944	14	69	0.950	8	76	0.921	4	80	0.942	8	69	0.940	8	69	0.900	24	90
Toravere	233	1368	0.941	-7	61	0.945	15	77	0.877	-2	80	0.941	-2	58	0.946	-1	56			
Val d'Alnya	308	637	0.923	42	95	0.940	114	123	0.894	40	110	0.939	38	80	0.940	51	84	0.838	94	143
Vaulx-en-Velin	266	1610	0.951	23	58	0.957	22	64	0.923	22	74	0.968	31	51	0.968	26	52	0.884	22	90
Wien	254	1570	0.931	-2	68	0.937	-6	73	0.920	-2	72	0.958	0	53	0.958	6	55	0.848	3	101
Yatir Forest	325	505	0.899	19	88	0.949	25	72	0.865	6	97	0.943	17	63	0.942	15	64	0.862	11	102
Zurich	259	1560	0.901	16	91	0.910	12	100	0.884	18	97	0.906	16	90	0.908	23	94	0.855	10	108
All sites	249	24096		12	67		22	75	12	80		20	60		19	61		19	95	

Intermediate sky conditions: first and second order statistics in absolute values for the global horizontal irradiance.
The sites in grey are not taken into account in the overall statistics.

	$G_h [\text{W/m}^2]$	nb	SolarGIS			Heliosat 3v3			3Tier			EnMetSol (Soilis)			EnMetSol (Dumontier)			IrSoIAV		
			R ²	mbd%	sd%	R ²	mbd%	sd%	R ²	mbd%	sd%	R ²	mbd%	sd%	R ²	mbd%	sd%	R ²	mbd%	sd%
Cabauw	252	1578	0.950	-4	22	0.951	0	24	0.919	0	27	0.970	1	17	0.968	0	17			
Camborne	249	1546	0.941	0	24	0.963	6	23	0.913	1	29	0.962	5	20	0.963	4	20			
Carpentras	267	986	0.937	8	26	0.966	15	26	0.929	4	26	0.964	13	21	0.965	15	22	0.779	10	51
Davos	235	1571	-2	43	43	0.948	26	35	0.861	7	43	0.887	-11	34	0.887	-5	37	0.693	-4	60
El Saler	304	1083	0.919	7	27	0.963	12	25	0.908	3	28	0.942	11	23	0.943	10	23	0.898	5	29
Geneva	266	1208	0.935	7	25	0.952	6	25	0.898	4	31	0.958	10	21	0.958	11	22	0.868	7	36
Jungfraujoch	270	1220	0.763	1	54	0.917	46	44	0.773	27	55	0.739	-24	45	0.734	-14	48	0.564	4	70
Las Majadas	292	1036	0.925	12	28	0.957	20	26	0.900	10	31	0.947	19	25	0.949	16	24	0.893	13	32
Lerwick	234	1307	0.933	0	24	0.937	8	31	0.870	6	35	0.938	-3	23	0.938	4	23			
Locarno	258	1199	0.944	9	25	0.958	19	31	0.928	12	30	0.963	14	22	0.962	13	22	0.901	9	33
Nantes	264	1595	0.958	-1	21	0.938	7	31	0.928	0	27	0.973	5	17	0.973	2	17	0.896	5	34
Payerne	247	1398	0.942	5	25	0.933	-1	29	0.904	4	32	0.957	8	23	0.957	10	24	0.867	4	37
Sede Boquer	274	522	0.931	11	27	0.946	2	28	0.878	1	32	0.944	10	25	0.944	7	24	0.900	9	32
Sion	224	1437	0.907	-1	33	0.964	28	33	0.905	10	34	0.953	5	25	0.950	4	26	0.771	1	52
Sonneblick	287	1570	0.765	3	54	0.901	37	44	0.777	19	55	0.767	-18	45	0.761	-5	49	0.661	10	64
Tamanrasset	313	915	0.954	13	25	0.962	30	35	0.921	18	36	0.956	25	31	0.957	24	30			
Thessaloniki	260	1036	0.944	5	26	0.950	3	29	0.921	2	31	0.942	3	26	0.940	3	26	0.900	9	35
Toravere	233	1368	0.941	-3	26	0.945	6	33	0.877	-1	34	0.941	-1	25	0.946	-1	24	0.838	30	46
Val d'Alnya	308	637	0.923	14	31	0.940	37	40	0.894	13	36	0.939	12	26	0.940	17	27	0.884	8	34
Wien	266	1610	0.956	8	22	0.957	8	24	0.923	8	28	0.968	12	19	0.968	10	19	0.884	1	40
Yatir Forest	325	505	0.899	6	27	0.949	8	22	0.865	2	30	0.943	5	19	0.942	5	20	0.862	3	31
Zurich	259	1560	0.901	6	35	0.910	5	39	0.884	7	37	0.906	6	35	0.908	9	36	0.855	4	42
All sites	249	24096		5	27		9	30	5	32		8	24		8	25		11	53	

Intermediate sky conditions: first and second order statistics in relative values for the global horizontal irradiance.
The sites in grey are not taken into account in the overall statistics.

Beam irradiance

Intermediate sky conditions $0.30 < K'_t \leq 0.65$

	B_n [W/m ²]	nb	SolarGis			Heliosat 3v3			3Tier			EnMetSol (Solis)			EnMetSol (Dumontier)			IrSoIAV			
			R2	mbd	sd	R2	mbd	sd	R2	mbd	sd	R2	mbd	sd	R2	mbd	sd	R2	mbd	sd	
Cabauw	122	1568	0.764	14	90	0.680	97	126	0.577	68	148	0.772	38	89	0.754	45	97	101	123	0.419	159
Camborne	104	1293	0.816	54	93	0.759	150	120	0.738	77	130	0.815	66	89	0.810	77	109	111	0.779	136	124
Carpentras	143	986	0.722	74	122	0.729	179	141	0.679	92	152	0.782	109	111	0.779	136	123	127	0.675	81	124
Davos	76	1571	0.561	111	161	0.566	245	162	0.557	149	191	0.688	24	90	0.675	81	127	0.474	123	127	197
El Saler																					
Geneva	153	1208	0.725	60	129	0.735	106	128	0.615	88	179	0.791	66	104	0.805	93	115	0.651	85	115	155
Jungfraujoch	14	1220	0.269	232	243	0.117	461	256	0.203	366	322	0.250	64	110	0.270	138	185	0.160	215	215	251
Las Majadas																					
Lerwick	82	1230	0.673	52	105	0.570	161	162	0.513	124	175	0.692	40	87	0.662	51	101				
Locarno																					
Nantes	163	1595	0.798	0	91	0.646	88	152	0.684	22	134	0.840	27	83	0.836	14	82	0.646	46	154	158
Payerne	111	1398	0.675	66	123	0.620	98	138	0.544	108	178	0.711	76	110	0.717	104	124	0.531	89	124	222
Sede Boquer	272	450	0.659	37	142	0.355	10	200	0.520	40	185	0.541	21	160	0.515	31	170	0.315	78	127	290
Sion	32	1570	0.401	216	250	0.402	419	242	0.395	308	293	0.451	57	112	0.490	148	189	0.391	262	173	290
Sonneblick	124	915	0.721	115	122	0.578	312	212	0.641	184	195	0.606	213	179	0.637	247	247				
Tamanrasset																					
Thessaloniki																					
Toravere	131	1368	0.733	3	108	0.726	106	148	0.411	75	193	0.633	21	125	0.694	38	122				
Val d'Alnya																					
Vaulx-en-Velin	206	1592	0.802	27	110	0.704	79	139	0.669	64	159	0.852	45	95	0.860	44	95	0.653	45	154	155
Wien	152	1570	0.748	24	114	0.748	74	127	0.674	61	149	0.804	26	96	0.792	57	109	0.633	51	127	155
Yatir Forest																					
Zurich																					
All sites	142	15173		40	110		119	146		81	163		58	108		72	114		73	171	

Intermediate sky conditions: first and second order statistics in absolute values for the normal beam irradiance.
The sites in grey are not taken into account in the overall statistics.

	B_n [W/m ²]	nb	SolarGis			Heliosat 3v3			3Tier			EnMetSol (Solis)			EnMetSol (Dumontier)			IrSoIAV			
			R2	mbd%	sd%	R2	mbd%	sd%	R2	mbd%	sd%	R2	mbd%	sd%	R2	mbd%	sd%	R2	mbd%	sd%	
Cabauw	122	1568	0.764	12	74	0.680	80	104	0.577	56	121	0.772	31	73	0.754	37	80				
Camborne	104	1293	0.816	52	90	0.759	144	115	0.738	74	125	0.815	63	86	0.810	74	97				
Carpentras	143	986	0.722	52	85	0.729	125	98	0.679	64	106	0.782	76	78	0.779	94	86	0.419	111	111	
Davos	76	1571	0.561	146	211	0.566	322	212	0.557	195	250	0.688	32	118	0.675	106	167	0.474	163	167	
El Saler																					
Geneva	153	1208	0.725	39	84	0.735	69	84	0.615	57	117	0.791	43	68	0.805	60	75	0.651	56	101	
Jungfraujoch	14	1220	0.269	1660	1743	0.117	3301	1833	0.203	2624	2311	0.250	461	790	0.270	988	1322	0.160	1542	1801	
Las Majadas																					
Lerwick	82	1230	0.673	64	129	0.570	197	198	0.513	151	214	0.692	49	107	0.662	62	124				
Locarno																					
Nantes	163	1595	0.798	0	56	0.646	54	93	0.684	13	82	0.840	17	51	0.836	9	50	0.646	28	94	
Payerne	111	1398	0.675	60	111	0.620	88	124	0.544	97	160	0.711	68	99	0.717	93	111	0.531	80	142	
Sede Boquer	272	450	0.659	14	52	0.355	4	74	0.520	15	68	0.541	8	59	0.515	11	62	0.315	29	82	
Sion	32	1570	0.401	93	99	0.578	252	171	0.641	149	158	0.606	172	145	0.637	200	140				
Sonneblick	124	915	0.721	2	82	0.726	81	113	0.411	57	147	0.633	16	96	0.694	29	93				
Tamanrasset																					
Thessaloniki																					
Toravere	131	1368	0.733	2	82	0.726	81	113	0.411	57	147	0.633	16	96	0.694	29	93				
Val d'Alnya	206	1592	0.802	13	53	0.704	38	67	0.689	31	77	0.852	22	46	0.860	22	46	0.653	22	75	
Wien	152	1570	0.748	16	75	0.748	49	84	0.674	40	98	0.804	17	63	0.792	38	72	0.633	34	102	
Yatir Forest																					
Zurich																					
All sites	142	15173	28	78		84	103		57	115		41	76		51	81		52	120		

Intermediate sky conditions: first and second order statistics in relative values for the normal beam irradiance. The sites in grey are not taken into account in the overall statistics.

Global irradiance

Overcast sky conditions

$$0.00 < K'_t \leq 0.30$$

Overcast sky conditions: first and second order statistics in absolute values for the global horizontal irradiance. The sites in grey are not taken into account in the overall statistics.

Location	G _h [W/m ²]	nb	Solar Gis			Heliostat 3v3			3Tier			EnMetSol (Solis)			EnMetSol (Dumortier)			I-Solar		
			R2	mber%	sd%	R2	mber%	sd%	R2	mber%	sd%	R2	mber%	sd%	R2	mber%	sd%	R2	mber%	sd%
Cabauw	79	1201	0.879	12	41	0.852	31	60	0.820	48	56	0.907	23	39	0.904	21	40			
Camborne	91	1179	0.866	9	43	0.897	43	65	0.848	34	49	0.888	22	41	0.900	22	40			
Carpentras	77	803	0.803	26	65	0.906	67	68	0.748	41	65	0.879	46	54	0.881	45	55	0.673	92	130
Davos	99	854	0.704	24	72	0.895	129	109	0.775	51	67	0.798	14	53	0.791	25	57	0.485	51	107
El Salter	86	490	0.697	31	79	0.803	48	74	0.627	66	106	0.789	49	71	0.789	47	71	0.594	47	89
Genesva	89	950	0.829	24	52	0.893	26	49	0.803	43	59	0.870	29	46	0.871	30	46	0.653	38	84
Jungfraujoch	105	533	0.632	73	123	0.900	184	147	0.668	141	122	0.611	25	81	0.594	44	93	0.467	97	170
Las Majadas	100	451	0.606	27	77	0.821	89	78	0.561	62	96	0.749	56	72	0.752	52	71	0.647	49	93
Lerwick	85	1125	0.868	31	49	0.873	53	83	0.792	56	64	0.834	20	48	0.839	19	48			
Locarno	64	1172	0.850	55	75	0.848	111	119	0.782	99	107	0.878	56	67	0.877	54	66	0.727	72	114
Nantes	96	1063	0.856	3	38	0.817	46	78	0.837	26	45	0.907	19	34	0.909	14	32	0.650	27	71
Payerne	88	1068	0.813	15	51	0.831	16	58	0.768	42	63	0.881	25	43	0.884	26	44	0.654	39	83
Sede Boquer	118	83	0.579	14	73	0.787	45	75	0.437	76	125	0.697	28	62	0.698	23	60	0.443	20	96
Sion	81	992	0.690	28	82	0.869	141	118	0.800	47	71	0.840	35	61	0.845	31	60	0.555	56	109
Tamanrasset	138	526	0.735	52	99	0.747	139	117	0.705	77	108	0.687	23	82	0.686	44	94	0.578	75	129
Thessaloniki	114	224	0.678	76	865	120	107	0.711	73	98	131	0.754	79	131	0.754	78	131			
Torrevieja	91	614	0.751	18	65	0.756	3	68	0.673	46	87	0.774	26	62	0.772	25	62	0.612	43	98
Val d'Albina	97	330	0.762	58	62	0.870	63	96	0.668	60	71	0.818	19	50	0.825	19	50			
Vaulx-en-Velin	86	1063	0.826	24	53	0.854	41	62	0.789	148	105	1.003	131	0.781	75	88	83	0.609	115	151
Wien	1203	1082	0.844	8	45	0.848	7	53	0.811	30	50	0.878	12	40	0.877	14	41	0.637	28	82
Yatir Forest	123	193	0.714	30	63	0.858	66	72	0.624	61	85	0.736	35	62	0.739	33	62	0.574	32	88
Zurich	91	1281	0.760	26	63	0.785	33	82	0.740	55	72	0.769	29	66	0.770	31	69	0.619	42	93
All sites	82	15917	22	60	48	80	51	75	30	58	29	59	29	59	29	59	63	63	138	

Overcast sky conditions: first and second order statistics in relative values for the global horizontal irradiance. The sites in grey are not taken into account in the overall statistics.